RSC Advances

PAPER

View Article Online
View Journal | View Issue

Cite this: *RSC Adv.*, 2025, **15**, 28666

High-performance corrosion inhibitors for carbon steel in hydrochloric acid: electrochemical and DFT studies

Qahtan A. Yousif, †*[a] Mahmoud A. Bedair, †*[b] Ahmed M. Abuelela,*[c] Azaj Ansari,[d] Sumit Sahil Malhotra[d] and Zainb Fadel[e]

This research examines the corrosion inhibition efficiency of two novel compounds, **AEPA** and **DOCA**, on carbon steel in 1.0 M hydrochloric acid. Both **AEPA** and **DOCA** demonstrated excellent electrochemical performance as corrosion inhibitors, with inhibition efficiencies exceeding 93% at a concentration of 10 mM, as confirmed through potentiodynamic polarization (PDP), electrochemical frequency modulation (EFM), and electrochemical impedance spectroscopy (EIS) techniques. EIS analysis revealed a marked increase in charge transfer resistance (R_{ct}), reaching 387.55 Ω cm^2 for **AEPA** and 345.80 Ω cm^2 for **DOCA**, indicating the formation of a robust protective layer on the carbon steel surface. Adsorption studies confirmed that both inhibitors follow the Langmuir isotherm model, suggesting monolayer chemisorption. The calculated adsorption equilibrium constants with corresponding Gibbs free energy values of −29.53 kJ per mol (**AEPA**) and −29.30 kJ per mol (**DOCA**), respectively, indicating spontaneous and strong adsorption interactions. Theoretical insights from density functional theory (DFT) calculations revealed that **AEPA** possesses a higher HOMO energy (−5.65 eV) and a lower LUMO energy (−1.12 eV) compared to **DOCA** (HOMO: −6.70 eV, LUMO: −0.85 eV), resulting in a smaller energy gap (ΔE = 4.53 eV for **AEPA** *vs.* 5.85 eV for **DOCA**). This suggests that **AEPA** has a greater electron-donating ability and stronger interaction with the metal surface. The integration of experimental and theoretical approaches provides a comprehensive understanding of their inhibition mechanisms and highlights their potential for practical applications in corrosion protection.

Received 10th July 2025
Accepted 7th August 2025

DOI: 10.1039/d5ra04952k

rsc.li/rsc-advances

1. Introduction

Corrosion is an inherent and often undesirable process that occurs when metals, like carbon steel, interact with their environment.[1] The most common form of deterioration, called rust in the case of iron and steel, results from the oxidation of the metal when it comes into contact with oxygen and moisture.[2] The deterioration of steel alloys has become a significant topic in academic and research fields because of its impacts on society and the economy.[3,4] Steel alloys are widely used in various industrial and construction applications.[5,6] Many devices rely on this material because of its affordability and strong structural properties.[7–9] Additionally, the acidic solutions used in various industrial processes, such as cleaning, scale removal, pickling, and oilfield acidizing, are highly corrosive, which accelerates the rate at which they corrode materials.[10–12] Consequently, corrosion of steel and other metals has become a common issue in today's industrial world.[13] Carbon steel is a fundamental building material widely used across various key industries, especially in the nuclear, petroleum, energy, food production, medical, chemical, and electrochemical sectors.[14–17] Carbon steel is vulnerable to specific types of corrosion in certain environments.[18] Hydrochloric acid (HCl) is often used as a corrosive solution in labs and industries due to its numerous benefits.[19,20] These include its high reactivity, integration (which is usually smart and widely available, making it a cost-effective choice), ease of use (which makes it simple to control and store, ideal for labs and factories), and effective reactivity for control.[21–23] The primary and most common methods to prevent corrosion include using surface coatings, developing the best metal alloys, utilizing pure metals, altering the environment, applying inhibitors, and employing cathodic protection.[6,19,24,25] Scientists are working on a wide range of chemical inhibitors to reduce metal corrosion.[26–29] The most effective inhibitors usually have many aromatic bonds and rings, along with nitrogen, sulfur, and oxygen.[30] However, traditional inhibitors have issues like

[a]*University of Al-Qadisiyah, College of Engineering, Department of Materials Engineering, Iraq. E-mail: qahtan.adnan@qu.edu.iq*

[b]*Department of Chemistry, College of Science, University of Bisha, P. O. Box 511, Bisha, 61922, Saudi Arabia. E-mail: m_bedier@yahoo.com; mbedair@ub.edu.sa*

[c]*Department of Chemistry, College of Science, King Faisal University, Al-Ahsa 31982, Saudi Arabia. E-mail: aabuelela@kfu.edu.sa*

[d]*Department of Chemistry, School of Basic Sciences, Central University of Haryana, Mahendergarh, Haryana, 123031, India*

[e]*General Directorate of Education Al-Qadisiyah, Ministry of Education, Iraq*

† Both authors contributed equally and considered as the first author.

toxicity.[31] As a result, research on environmentally friendly and sustainable corrosion inhibitors has mainly focused on chemicals that are cheaper, more effective, and less harmful to the environment.[32–34] The most common synthetic corrosion inhibitors are heterocyclic organic compounds with conjugated double bonds, polar functional groups, and more electronegative atoms such as sulfur, nitrogen, phosphorus, and oxygen.[35,36]

In our recent studies, we have explored a wide range of organic compounds as corrosion inhibitors for steel in acidic environments. We reported penicillanic acid derivatives CDOT and IDOT achieving inhibition efficiencies of 95.51% and 95.14%, respectively, with adsorption energies of −39.2 and −37.8 kJ mol^{-1}, indicating strong chemisorption.[37] Similarly, we synthesized DOP and ADO, which reached efficiencies of 80.76% and 72.49% at 10 mM, supported by SEM/EDX and DFT analyses.[38] We also introduced tri-thiosemicarbazones HBC and HAC, achieving up to 98.8% efficiency and R_{ct} values of 4930 Ω cm^2, with Monte Carlo simulations confirming strong surface interactions.[39] In another study, we evaluated benzimidazole derivatives (BIT, BIY, BIH) with efficiencies up to 93.43%, while a coumarin-based surfactant reached 97.93% efficiency and ΔG_{ads} values around −38.6 kJ mol^{-1}. In our green chemistry approaches, we used bellerica extract, achieving 91.79% efficiency, with DFT band gaps ranging from 4.81 to 7.56 eV.[40]

Schiff bases have a broad range of uses, especially in medicine and pharmacology, where they serve as corrosion inhibitors and exhibit properties like analgesic, anti-inflammatory, antibacterial, anticancer, and antioxidant effects.[41] Researchers have performed many studies on new Schiff base derivatives to enhance their inhibitory efficiency.[9,42] Schiff bases are created through condensation, which happens when an amine or aldehyde reacts with a ketone.[43] They provide better corrosion inhibition than other aldehydes and amines of a similar type because Schiff bases contain the $R_1N{=}CR_2R_3$ group.[32,44,45] The derivatives of 6-amino penicillinic acid and 4-amino acetophenone are effective at preventing corrosion. These compounds contain polar groups that help them adhere better to metal surfaces, especially under harsh conditions. Additionally, the many π-electrons and lone electron pairs in the oxygen and nitrogen atoms interact with the d-orbitals of metal to form a protective layer. Two novel compounds, (*S*,*E*)-2-((1-(4-minophenyl)ethylidene)amino) (3-(4-hydroxyphenyl)propanoic acid), "**AEPA**", and (2*S*,5*R*,6*R*)-3,3-dimethyl-7-oxo-6-propionamido-4-thia-1-azabicyclo[3.2.0] heptane-2-carboxylic acid, "**DOCA**", are synthesized. The critical improvement of this work lies in the synergistic integration of experimental electrochemical techniques with advanced quantum chemical modeling, providing a deeper mechanistic understanding and predictive capability for corrosion inhibition. This positions **AEPA** and **DOCA** as next-generation inhibitors with both practical and theoretical significance in the field of corrosion science.

2. Methodologies

2.1. Materials and instruments

This investigation used high-quality Sigma-Aldrich 6-amino penicillinic acid, propanoyl chloride, tyrosine, and ethyl acetate. The Scharlau Company supplied sodium hydrogen carbonate and hydrochloric acid. The IR spectra were taken using potassium bromide discs on a Shimadzu "FTIR-8400S" spectrophotometer, ranging from 400 to 4000 cm^{-1}. Compound electronic spectra were measured with a Shimadzu "UV-1800" spectrophotometer. The ^1H and ^{13}C nuclei were mixed with D_2O for analysis on a Bruker "DPX-300" NMR spectrometer. The ^{13}C and ^1H NMR spectra were recorded at frequencies of 150 and 600 MHz, respectively, using a method to reduce interference from ^1H nuclei. The Flash EA112 elemental analyzer was used to analyze carbon, hydrogen, and nitrogen. After immersing carbon steel samples in 1.0 M hydrochloric acid, with or without **AEPA** and **DOCA**, their surface microstructure was examined using a ZEISS Sigma FESEM. Images were captured for EDX analysis, and maps were created for further analysis.

2.2. Synthesis of DOCA and AEPA inhibitors

Propanoyl chloride (1 mmol) was mixed with 30 mL of acetone and then added to a solution containing 1 mmol of 6-amino penicillinic acid dissolved in 40 mL of a 2% sodium bicarbonate solution. The mixture was stirred for 2 to 4 hours at zero degrees celsius. Afterwards, the solution was concentrated by evaporation. The water layer was then acidified with 0.1 M hydrochloric acid, and the solid was extracted using 25 mL of ethyl acetate.[46] It was washed with distilled water and dried over anhydrous Na_2SO_4. The ethyl acetate was evaporated, and the resulting precipitate was collected. The melting point of the synthesized **DOCA** was then measured (Scheme 1). But for the **AEPA** compound, follow these steps: dissolve 1 mmol of 4-aminoacetophenone in 10 mL of methanol with continuous stirring until fully dissolved. Then, add two drops of glacial acetic acid as a catalyst. Next, dissolve 1 mmol of the amino acid tyrosine in 15 mL of methanol. Slowly add the amino acid solution to the aromatic ketone (Scheme 2).[34] Heat the mixture at 65 °C in a water bath for 8 to 10 hours. After cooling, filter the precipitate, wash it with methanol, and air-dry for two hours.

2.3. Corrosion inhibition methodology

The composition of the carbon steel samples (weight percentage) included C (0.18%), Mn (1.40%), Si (0.36%), Ni (0.04%), Cu (0.33%), Cr (0.02%), Mo (0.02%), and Fe (balanced). Precise measurements were necessary for constructing the working electrode. Mechanical methods were used to obtain uniform sizes with a thickness of approximately 1 cm. The exposed area of 1 cm^2 was manually abraded before applying epoxy glue to cover the parts. Distilled water was used to thoroughly clean the electrode, and acetone and hot benzene were employed to remove grease, followed by drying at room temperature. Electrochemical experiments were conducted at 30 °C using a potentiostat, and the data were analyzed with appropriate software. In the electrochemical cell, the working electrode was made of carbon steel, the reference electrode was a mercury–mercury sulfate electrode, and the counter electrode was a platinum plate. All three electrodes were fully immersed in a 1.0 M hydrochloric acid solution. To ensure a stable open circuit potential (OCP), the carbon steel sample was subjected to spontaneous corrosion for

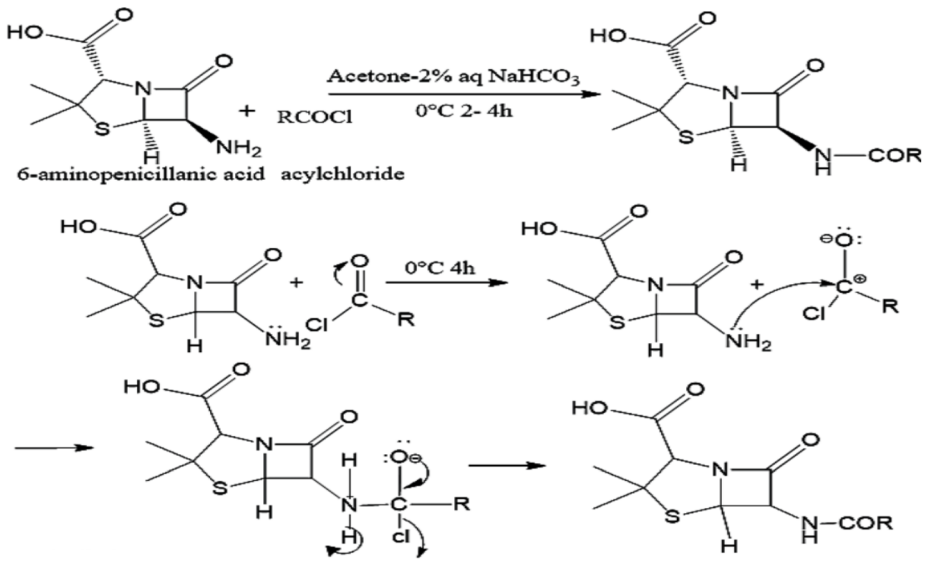

Scheme 1 Synthetic pathway and the suggested mechanism of **DOCA** inhibitor.

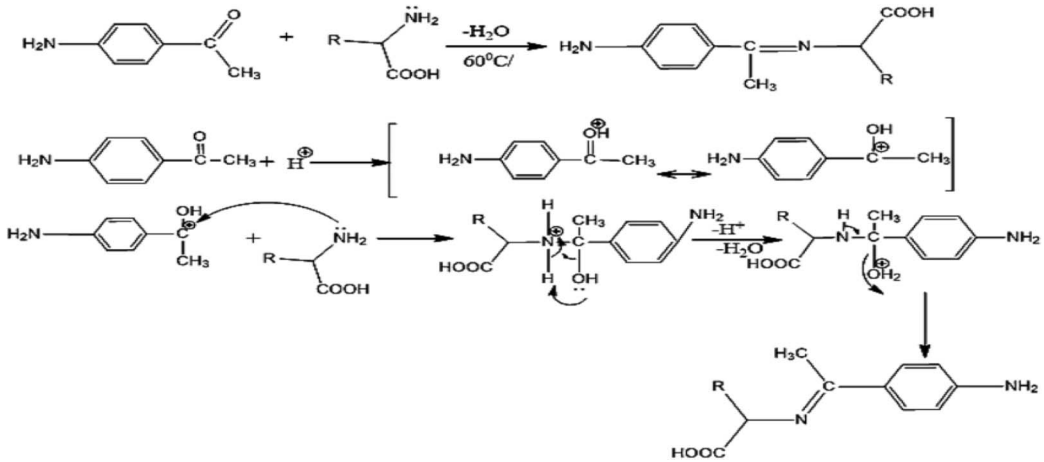

Scheme 2 Synthetic pathway and the suggested mechanism of **AEPA** inhibitor.

30 minutes before the experiments without applying any external current or voltage. The electrochemical impedance spectroscopy (EIS) and potentiodynamic polarization (PDP) methods used in this study were previously described in our research. The experiments were conducted with and without **DOCA** and **AEPA** inhibitors. The electrochemical potentials of carbon steel samples were measured using the PDP method, which involves a scan rate of 2 mV s^{-1} and a potential range of ±0.6 V. Eqn (1) presents all the electrochemical parameters used to evaluate the inhibitory efficiency derived from Tafel plots for the polarization study. Eqn (1) shows the inhibition efficiency (η_p %) which compares the corrosion current densities with (i_{corr}) and without (i^0_{corr}) the presence of **DOCA** and **AEPA**.

$$\eta_p\% = 100\left(1 - \frac{i_{corr}}{i^0_{corr}}\right) \quad (1)$$

The impedance test, with amplitude of ±10 mV, utilized a frequency response range of 1 Hz to 100 kHz. A similar design was employed to match the impedance range. It is important to clearly understand the charge transfer resistance (R_{ct}), solution resistance (R_s), and inhibition efficiency (η_z %). Bode and Nyquist plots were used to illustrate the impedance range. Using the provided data, eqn (2) was applied to calculate the corrosion inhibition rate, which is (η_z %). The charge transfer resistances for both **DOCA** and **AEPA** inhibitors (R_{ct}) and in the absence of these inhibitors (R^0_{ct}) are presented.

$$\eta_z\% = 100\left(\frac{R_{ct} - R^0_{ct}}{R_{ct}}\right) \quad (2)$$

The electrochemical frequency modulation (EFM) requirements are satisfied with a potential disturbance signal that has an amplitude of 10 mV. It consists of two sine waves at 0.2 and 0.5 Hz, totaling 16 cycles. The full parameters are determined using the most prominent peaks. Eqn (3) can be used to calculate the efficiency (η_{EFM} %).

$$\eta_{EFM}\% = 100\left(1 - \frac{i_{corr}}{i^{0}_{corr}}\right) \quad (3)$$

To ensure the data obtained were accurate, electrochemical experiments were conducted for each concentration of **DOCA** and **AEPA** inhibitors.

2.4. Computational methods

To explore the electronic structure and reactivity of the studied organic molecules, we employed density functional theory (DFT) calculations using the unrestricted B3LYP functional with the 6-31G basis set implemented in Gaussian 16 package.[47] Solvent effects were incorporated using the polarizable continuum model (PCM) with water as the solvent, specified *via* the scrf=(solvent=water) keyword. To simulate acidic environments, we protonated the molecules by adding a hydrogen atom near the amino group, which is a likely site of protonation under such conditions. Geometry optimizations were performed using the geom=connectivity keyword, and Hirshfeld population analysis (pop=hirshfeld) was used to evaluate charge distribution. The calculations were carried out with a maximum disk allocation of 8 GB to ensure computational efficiency. Both alpha and beta spin molecular orbitals were analyzed to capture the full spin-resolved electronic structure. However, for consistency and clarity in comparing frontier molecular orbitals (FMOs), we focused on the beta spin orbitals when reporting HOMO and LUMO energies. The HOMO–LUMO gap, along with the individual orbital energies, was used to assess the chemical reactivity of the investigated inhibitors. Finally, we calculated the density of states (DOS) using GaussSum software.[48] To simplify the visual representation, hydrogen atoms were excluded from the images.

3. Results and discussion

3.1. DOCA and AEPA inhibitor characterization

3.1.1. Chemical and physical properties of DOCA and AEPA inhibitors. We examined the physicochemical properties of **DOCA** and **AEPA** inhibitors, including their color, melting point, and elemental composition. The **DOCA** compound appears as a yellowish-white powder. It has a melting point range of 206–208 °C and an 82% yield. The **AEPA** compound melts between 210 and 212 °C and has a 93% yield. The **AEPA** compound also has an orange color. **DOCA** contains 9.71% nitrogen, 33.11% carbon, 17.24% sulfur, and 2.99% hydrogen. **AEPA** consists of 4.37% nitrogen, 38.20% carbon, and 4.55% hydrogen.

3.1.2. FT-IR analysis. Compound **DOCA** (Fig. 1) showed a significant spectrum: a broad absorption band at 3300 cm^{-1} due to the stretching of the (O–H) bond of the carboxylic acid, and an absorption band at 780 cm^{-1} due to the stretching of the (C–S) bond. It also showed an absorption band at 2960 cm^{-1} due to the stretching of the (sp^3C–H) bond. Additionally, it exhibited an absorption band at 1631 cm^{-1} due to the stretching of the (C=O) bond of the amide, and a band at 1713 cm^{-1} due to the stretching of the beta-lactam (C=O). A band at

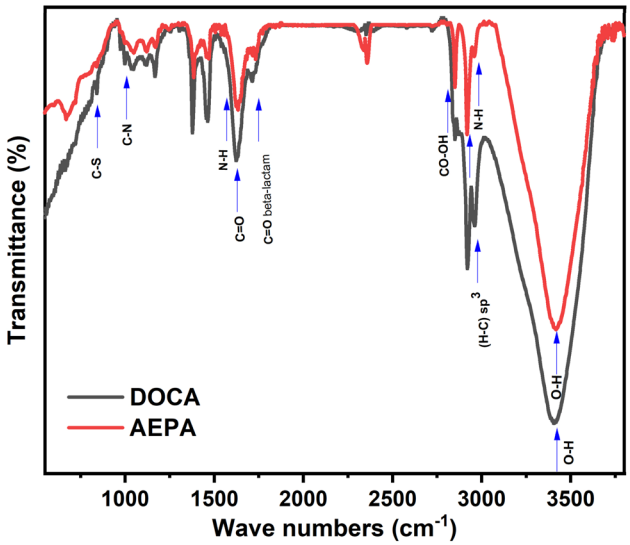

Fig. 1 FT-IR spectra of the investigated inhibitors (DOCA and AEPA).

973 cm^{-1} due to the stretching of the (C–N) bond of the amide, and an absorption band at 998 cm^{-1} due to the stretching of the (C–O) bond of the acid. Likewise, compound **AEPA** (Fig. 1) displayed a broad absorption band at 1973 cm^{-1}. The band at 3209 cm^{-1} is due to the bending of the alcoholic (O–H) bond, while a broad absorption band at 3394 cm^{-1} results from the bending of the amino (N–H) bond. Additionally, a broad band at 3116 cm^{-1} corresponds to the bending of the (CO–OH) group in the carboxylic acid, and an absorption band at 1635 cm^{-1} is due to the bending of the (C=N imine group). An absorption band at 1900 cm^{-1} reflects the bending of the (C=O) bond in the carboxylic acid. For bending vibrations, the compound exhibits a band at 1650 cm^{-1}, a band due to the bending of the amino (N–H) bond, absorption at 1357 cm^{-1} from the bending of the alcoholic (O–H) bond, and another at 1434 cm^{-1} due to the (O–H) bending of the carboxylic acid. The **AEPA** compound also shows an absorption band at 2968 cm^{-1} attributable to the (sp^3C–H) bond, and another at 1731 cm^{-1} due to the (C=N) bond.

3.1.3. ^{1}H and ^{13}C NMR analysis. The ^{1}H and ^{13}C NMR spectra are shown in Fig. 2 and 3. The ^{1}H NMR spectrum of the **DOCA** molecule in deuterium oxide (D_2O) displayed clear signals at specific chemical shifts (δ) in parts per million (ppm). These signals appeared at δ = 4.2 (C–H2, singlet), 1.56 (C–H12 and C–H18, singlet), 5.5 (C–H6, doublet), 4.9 (C–H19, doublet), and 1.44 (C–H13 and C–H17, doublet). The **AEPA** molecule exhibits distinct signals at δ (ppm) = 3.4 (singlet, C–H15), 3.9 (doublet, C–H3), 4.7 (singlet, C–H2, C–H12, C–H17, C–H21, and C–H22), 5.8 (singlet, C–H17, C–H8, C–H10, and C–H20), and 7.8 (multiple, C–H11 and C–H7). Furthermore, as shown in Fig. 3, the ^{13}C NMR (D_2O) spectra of **DOCA** and **AEPA** displayed distinct signals at δ (ppm) = 26 (C12), 30 (C17 and C18), 73 (C5 and C2), and 56 (C6 and C3) for **DOCA**. The **AEPA** shows chemical shifts of 114 for (C20, C218, C10, and C8) and 131 for (C21, C17, C11, C7, and C6).

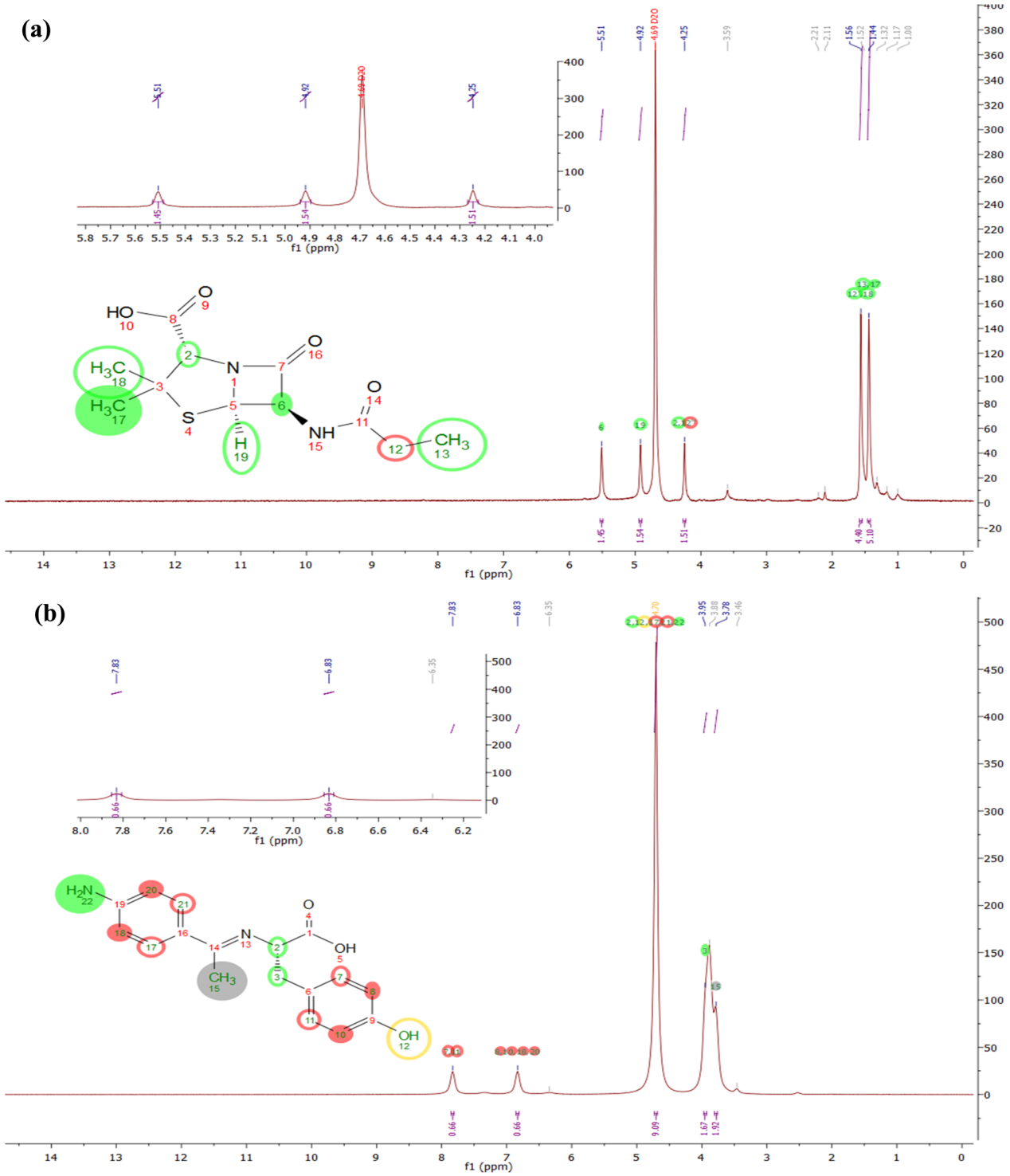

Fig. 2 ^{1}H NMR spectra of the investigated inhibitors (**DOCA** (a) and **AEPA** (b)).

3.1.4. UV-visible analysis. To determine the UV-visible spectra of **DOCA** and **AEPA**, a wavelength range of 200–600 nm was used for measurement. Quantification of the **DOCA** and **AEPA** compounds was performed in the lab at room temperature, with concentrations from 3.5×10^{-4} M. Fig. 4 shows the UV spectrum of compound **DOCA**. The strongest absorption occurs near 228 nm, while the weakest is at 216 nm. This is due to n–π* and π–π* electronic transitions. It is clear that a carbonyl group (C=O) exists in the lactam ring, along with heteroatoms such as nitrogen and sulfur. The hypochromic effect causes the change in absorbance intensity. Fig. 4 also displays the UV spectrum of compound **AEPA**. The peak maximum is at $\lambda_{max} = 229$ nm, with additional peaks at 247 nm and 361 nm. These peaks result from n–π* and π–π* electronic

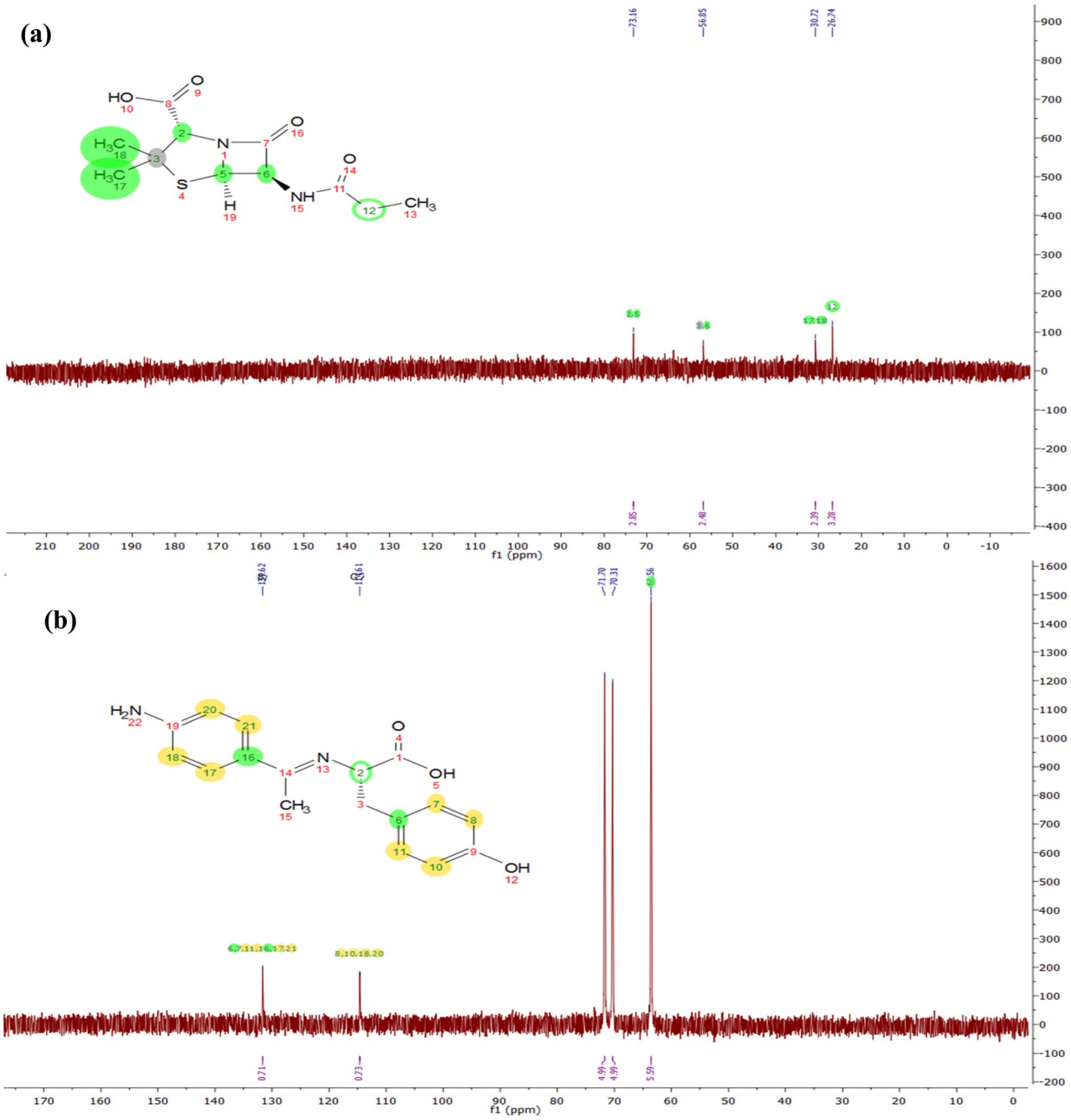

Fig. 3 ^{13}CNMR spectra of the investigated inhibitors (**DOCA** (a) and **AEPA** (b)).

transitions of the imine group (C═N) and aromatic ring transitions.

3.2. Electrochemical measurements

3.2.1. Potentiodynamic polarization. The electrochemical behavior of carbon steel in 1.0 M HCl solution in the presence of varying concentrations (0–10 mM) of **AEPA** and **DOCA** has been investigated using potentiodynamic polarization (PDP). The resulting electrochemical parameters like corrosion current density (i_{corr}), corrosion potential (E_{corr}), Tafel slopes (β_a, β_c), corrosion rate (k), surface coverage (θ), and inhibition efficiency (η) are collected in Table 1, and polarization curves are given in Fig. 5. In the absence of inhibitors, the density of the corrosion current (i_{corr}) was found to be 684 μA cm^{-2}, indicating a rapid dissolution of carbon steel in strongly acidic media.[49] However, the addition of **AEPA** and **DOCA** significantly decreased i_{corr}, demonstrating their effectiveness as corrosion inhibitors. With the concentration of 1 mM, the i_{corr} value fell to 167 μA cm^{-2} for **AEPA** and 168 μA cm^{-2} for **DOCA**. Increasing the concentration further to 10 mM caused a notable drop to 65.5 μA cm^{-2} and 67.7 μA cm^{-2} for both compounds. The trend agrees with that of earlier studies on organic corrosion inhibitors, in which the

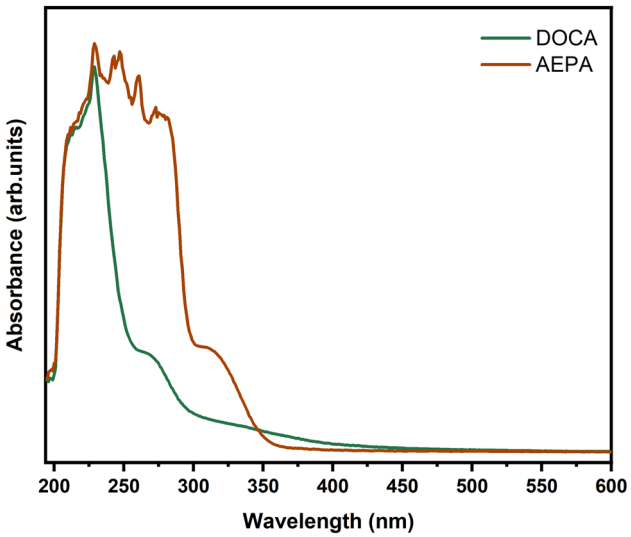

Fig. 4 UV spectra of the investigated inhibitors (DOCA and AEPA).

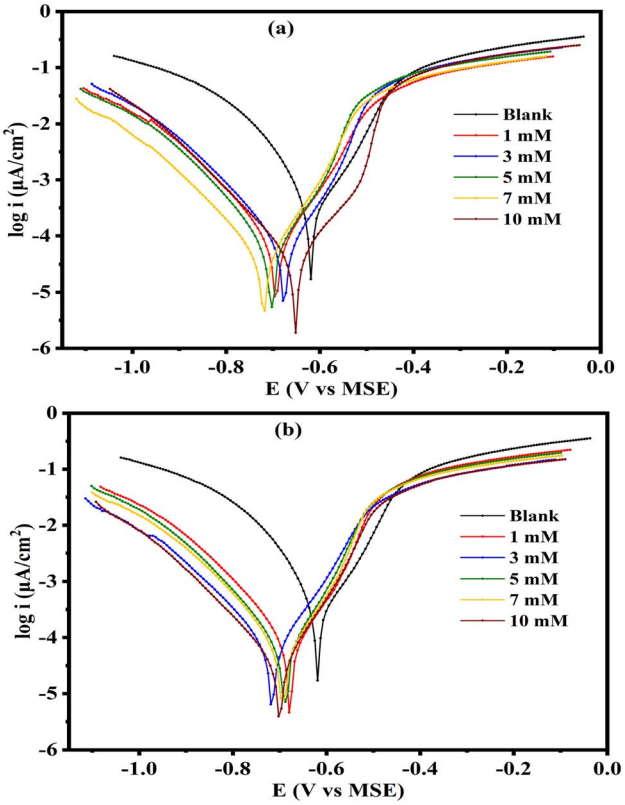

Fig. 5 Potentiodynamic polarization curves for the corrosion of carbon steel in 1.0 M HCl in absence and presence of different concentrations of AEPA (a) and DOCA (b) compounds at 30 °C.

higher inhibitor concentrations favor greater surface coverage *via* enhanced adsorption processes.[50–52] The corrosion potential (E_{corr}) moved to more negative values with the addition of both inhibitors, indicating a prevailing control over the cathodic reaction. In particular, at 10 mM concentration, E_{corr} shifted from −630 mV *vs.* MSE in blank solution to −653 mV *vs.* MSE and −700 mV *vs.* MSE for both **AEPA** and **DOCA**. The cathodic shift indicates that the inhibitors function primarily to suppress hydrogen evolution by forming a barrier on the cathodic sites of the metal surface.[53,54] The anodic (β_a) and cathodic (β_c) Tafel slopes were slightly changed at all the concentrations examined, showing that the mechanisms of hydrogen evolution and iron dissolution were not altered in the presence of the inhibitors.[11,55] Instead, the decrease observed in i_{corr} can be explained by physical blocking of the active sites on the metal surface through inhibitors' adsorption.[56] The measured corrosion rates had the same trend as that of i_{corr} as the value reduced from 360.5 mpy in the blank solution to 34.52 mpy and 35.65 mpy at 10 mM concentration for both **AEPA** and **DOCA**. These results further validate the strong inhibitory effect displayed by the investigated compounds. Surface coverage (θ) increased with increasing inhibitor concentration to a maximum of 0.904 at 10 mM corresponding to an inhibition efficiency of 90.42%. The high inhibition efficiency is a pointer to the ability of **AEPA** and **DOCA** to effectively cover the reactive surface and inhibit the

Table 1 Electrochemical parameters[a] for carbon steel dissolution in 1.0 M HCl solution containing different concentrations of the (AEPA and DOCA) inhibitors obtained from polarization measurements at 30 °C

Inhibitor name	Conc. (mM)	E_{corr} *vs.*.MSE (mV)	i_{corr} (μA cm^{-2})	β_a (mV dec^{-1})	$-\beta_c$ (mV dec^{-1})	R_p Ω cm^2	k (mpy)	θ	η_p %
Blank	—	−630	684	189.1	176.9	58.02	360.5	—	—
AEPA	1	−694	167	182.9	161.4	222.93	87.72	0.756	75.58
	3	−676	137	170.0	151.9	254.26	72.16	0.800	79.97
	5	−703	121	172.1	151.3	288.94	63.51	0.823	82.31
	7	−720	83.5	170.3	155.2	422.26	48.99	0.878	87.79
	10	−653	65.5	157.7	137.8	487.52	34.52	0.904	90.42
DOCA	1	−679	168	177.3	154.4	213.31	88.37	0.754	75.44
	3	−717	144	184.5	167.9	265.07	75.85	0.789	78.95
	5	−689	131	171.7	151.3	266.59	68.84	0.808	80.85
	7	−694	119	174	153.2	297.27	62.90	0.826	82.60
	10	−700	67.7	149.9	167.4	507.23	35.65	0.901	90.10

[a] E_{corr}, is the corrosion potential; i_{corr}, is the corrosion current density: β_a and β_c are Tafel constants for both anode and cathode; k, is the corrosion rate; θ, is the surface coverage; η_p, is the inhibition efficiency.

corrosion process.[57] **DOCA** and **AEPA** exhibited high electrochemical inhibition behavior, possibly owing to the presence of electron-rich nitrogen and sulfur atoms, which result in extensive interaction with the metal interface *via* chemisorption or coordination bonding.[58] The presence of these functional groups facilitates the adsorption ability of the molecules, resulting in the creation of a stable protective layer.[59] In general, the results of PDP analysis confirm that **AEPA** and **DOCA** are effective mixed-type inhibitors, the action of which is mainly on the cathodic reaction path. They perform better with an increase in concentration to achieve outstanding inhibition efficiencies greater than 90%.

3.2.2. Electrochemical frequency modulation. In order to further elucidate the corrosion inhibition mechanism of **AEPA** and **DOCA** for carbon steel in 1.0 M HCl solution, electrochemical frequency modulation (EFM) tests were carried out. EFM is a highly effective non-destructive technique in which the corrosion current density (i_{corr}), causative factors (CF-2 and CF-3), and intermodulation spectra measured without prepolarization of the electrode.[34] The resulting (EFM) spectra are presented in Fig. 6 for **AEPA**, whereas the respective electrochemical parameters obtained from these measurements are listed in Table 2. For the case without inhibitors (blank solution), the spectrum exhibited high current amplitude for the whole frequency range, suggesting active dissolution of carbon steel through vigorous acid attack.[60] Introduction of **AEPA** and **DOCA** brought about a remarkable decrease in the intermodulation current response with increasing concentration of the inhibitors, indicating gradual improvement in surface coverage and improved protection. Both compounds produced a significant reduction in current amplitude at a concentration of 1 mM, which signals the start of adsorption and partial inhibition. In 5–10 mM, the spectra were significantly flattened, particularly at lower frequencies, revealing the formation of a thick protective film that highly suppressed charge transfer processes at the metal/solution interface.[60,61] In Table 2, i_{corr} value in the blank solution, was 451.1 μA cm^{-2}. The introduction of **AEPA** and **DOCA** resulted in a consistent reduction from this value. At 10 mM, i_{corr} decreased to 30.6 μA cm^{-2} for **AEPA** and 31.7 μA cm^{-2} for **DOCA**. These decreases confirm the effectiveness of both compounds in reducing the general rate of corrosion by creating a protective film on the metal surface.[62] Both the cathodic and anodic Tafel slopes showed regular behavior over varying concentrations, *i.e.*, the mechanisms of iron dissolution and hydrogen evolution were not changed. Changes in β_c and β_a values, propose to have an influence on the cathodic and anodic reaction mechanism, most probably through physical blocking of active sites by inhibitor molecules that are adsorbed.[63] Both

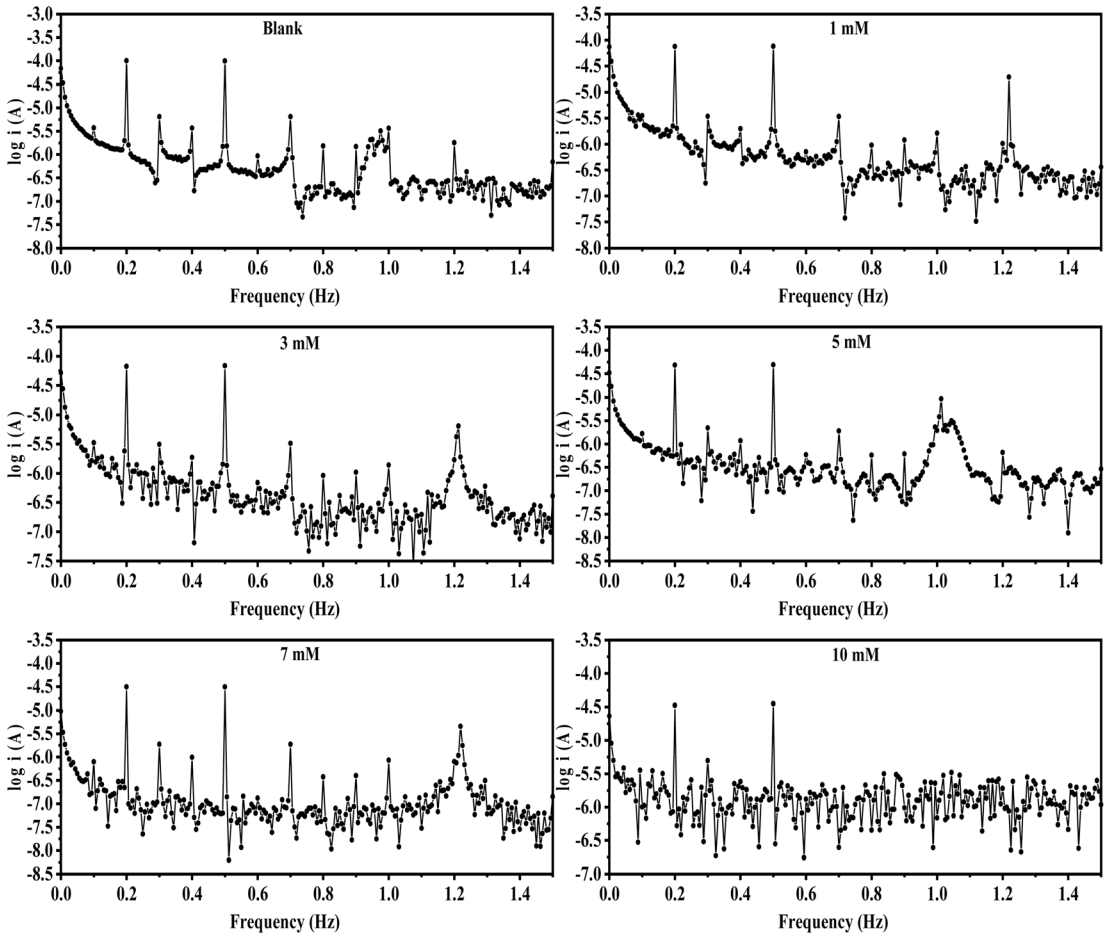

Fig. 6 Intermodulation spectra for carbon steel in 1.0 M HCl in absence and presence of different concentrations from AEPA compound at 30 °C.

Table 2 Electrochemical kinetic parameters[a] obtained by EFM technique for carbon steel in the absence and presence of various concentrations of (AEPA and DOCA) inhibitors in 1.0 M HCl at 30 °C

Inhibitor name	Conc. (mM)	i_{corr} (μA cm^{-2})	β_a (mV dec^{-1})	$-\beta_c$ (mV dec^{-1})	CF-2	CF-3	R_p μΩ	k (mpy)	θ	η_{EFM} %
Blank	—	451.1	38.45	68.73	1.826	2.909	34.08	209.1	—	—
AEPA	1	82.3	71.52	89.82	1.899	3.129	210.1	38.1	0.818	81.76
	3	67.6	66.88	83.38	1.967	3.174	246.7	31.3	0.850	85.01
	5	60.2	79.19	100.00	1.986	3.302	318.6	27.9	0.867	86.65
	7	38.3	75.49	105.40	2.040	3.324	407.4	17.8	0.915	91.51
	10	30.6	58.84	82.21	1.691	2.903	498.5	14.2	0.932	93.22
DOCA	1	93.3	80.68	94.75	1.843	2.457	202.9	43.2	0.793	79.32
	3	68.0	105.50	128.20	2.144	2.797	238.4	31.5	0.849	84.93
	5	62.6	65.00	78.57	1.469	2.490	304.3	29.0	0.861	86.12
	7	56.5	65.89	99.31	1.952	3.151	369.6	26.2	0.875	87.48
	10	31.7	54.02	65.94	1.881	2.948	487.3	14.7	0.930	92.97

[a] E_{corr}, is the corrosion potential; i_{corr}, is the corrosion current density: β_a and β_c are Tafel constants for both anode and cathode; k, is the corrosion rate; θ, is the surface coverage; η_{EFM}, is the inhibition efficiency.

CF-2 and CF-3 values were within the theoretical limit of ±10% throughout, ensuring the accuracy of EFM measurements. The slight deviations of CF values with rising concentration may indicate a shift in the dominant electrochemical mechanism in accordance with the nature of inhibition and adsorption behavior.[46,64] Surface coverage was increased by inhibitor concentration up to a maximum of 0.932 for **AEPA** and 0.930 for **DOCA** at 10 mM. These were equivalent to inhibition efficiencies of 93.22% and 92.97%, respectively, confirming the good inhibitory performance of the two compounds.[65] The noted decrease in i_{corr} and the rise in surface coverage provides powerful evidence for an inhibition mechanism through adsorption. The fact that **AEPA** and **DOCA** contain electron-rich nitrogen and sulfur atoms enables them to coordinate strongly with the iron surface *via* chemisorption or electrostatic attraction.[66] The reaction therefore results in the creation of a stable adsorbed layer, which suppresses both anodic and cathodic reactions and hence lowers the overall rate of corrosion.[67] The EFM results affirm that **AEPA** and **DOCA** are good corrosion inhibitors of carbon steel in 1.0 M HCl solution. These findings validate the results of potentiodynamic polarization studies and reveal that **AEPA** and **DOCA** show potential for practical applications in the inhibition of acid corrosion.

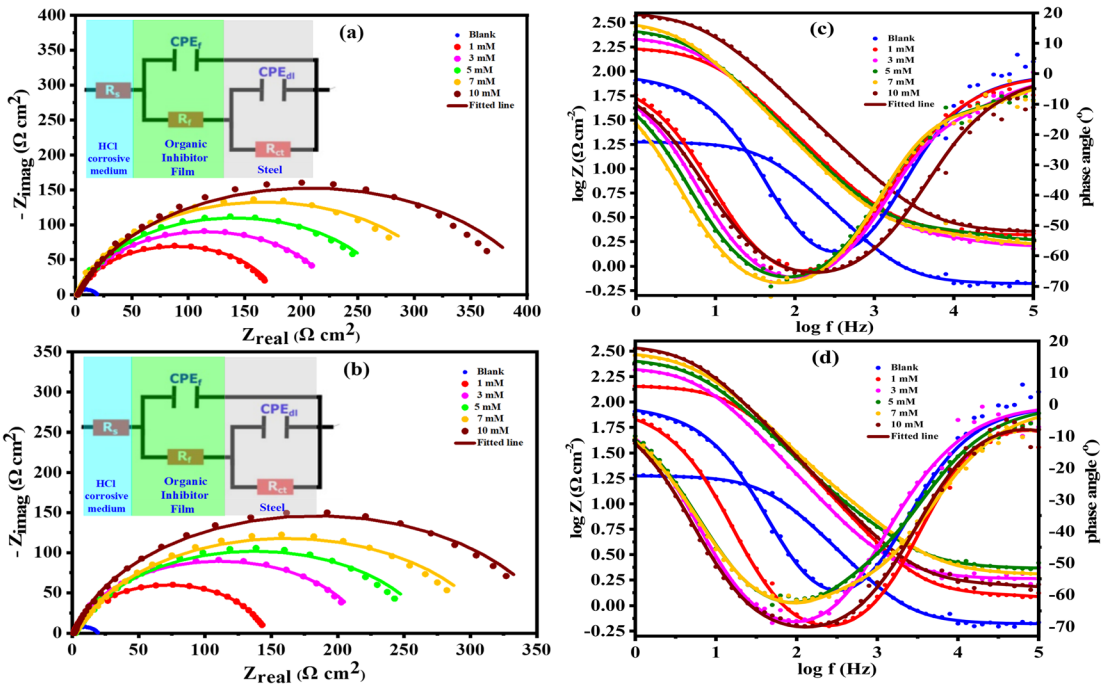

Fig. 7 Nyquist plots, Bode and phase angle plots for steel in 1.0 M HCl solution without and with different concentrations of AEPA (a and c), and DOCA (b and d) compounds at 30 °C.

Table 3 EIS parameters for corrosion of steel in 1.0 M HCl in the absence and presence of different concentrations of (**AEPA** and **DOCA**) inhibitors at 30 °C[a]

Inhibitor	Conc. (mM)	R_s (Ω cm^2)	R_f (Ω cm^2)	CPE_f		C_f (mF cm^{-2})	R_{ct} (Ω cm^2)	CPE_{dl}		C_{dl} (μF cm^{-2})	Chi squared (χ^2)	R_p ($R_f + R_{ct}$)	θ	η_z %
				Y_{o1} (m Ω^{-1} s^n cm^{-2})	n_1			Y_{o2} ($\mu\ \Omega^{-1}$ s^n cm^{-2})	n_2					
Blank	—	1.066					18.30	374.50	0.8752	184.02	3.15×10^{-3}	18.30	—	—
AEPA	1	2.0699	4.091	179.75	0.8374	44.28	171.62	166.10	0.9987	165.33	8.45×10^{-4}	175.71	0.8958	89.58
	3	1.5820	7.074	149.85	0.8902	64.38	219.79	134.16	0.8393	68.33	7.46×10^{-4}	226.86	0.9193	91.93
	5	1.7898	10.997	67.648	0.8623	21.41	266.81	115.77	0.8503	62.76	1.41×10^{-3}	277.80	0.9341	93.41
	7	1.6251	16.017	52.93	0.8483	14.94	314.45	18.66	0.8691	8.60	2.15×10^{-3}	330.47	0.9446	94.46
	10	2.2114	22.590	1.4313	0.8148	0.14	387.55	7.60	0.9999	7.60	1.91×10^{-3}	410.14	0.9554	95.54
DOCA	1	1.5134	5.802	192.50	0.8007	35.45	138.93	198.23	0.8994	132.64	6.39×10^{-4}	144.73	0.8736	87.36
	3	1.8197	6.513	151.55	0.8607	49.44	211.84	135.86	0.9999	135.81	4.05×10^{-3}	218.35	0.9162	91.62
	5	2.2962	8.203	108.00	0.8179	22.58	261.27	128.93	0.8673	76.74	1.04×10^{-3}	269.48	0.9321	93.21
	7	1.9926	14.698	57.16	0.8013	9.87	302.96	33.41	0.9229	22.76	8.80×10^{-4}	317.65	0.9424	94.24
	10	0.9777	19.640	4.97	0.8624	1.14	345.80	9.40	0.8594	3.68	1.91×10^{-3}	365.44	0.9499	94.99

[a] R_s = solution resistance, R_{ct} = charge transfer resistant, Y_o, n = constant phase elements, C_{dl} = double layer capacitance, θ = surface coverage, η_z = inhibition efficiency.

3.2.3. Electrochemical impedance spectroscopy. Electrochemical impedance spectroscopy (EIS) was used to examine the corrosion inhibition performance of **AEPA** and **DOCA** for carbon steel in 1.0 M HCl solution. EIS gives useful information about the protective ability of inhibitors through measurement of the impedance behavior of the metal/solution interface across a wide frequency range.[8,68] Fig. 7 represents the Nyquist plots, the Bode modulus and phase angle plots of **AEPA** and **DOCA**; in addition to this, the related EIS parameters are given in Table 3. In the absence of inhibitors (blank solution), the Nyquist plot (Fig. 7a and b) consisted of one capacitive loop with a relatively low charge transfer resistance (R_{ct}). This suggests the presence of active corrosion mechanisms due to the aggressive acid environment, in which the dissolution of carbon steel is not greatly inhibited.[69] At the minimum concentration of 1 mM **AEPA**, the Nyquist plot (Fig. 7a) revealed a noticeable increase in the diameter of the capacitive loop with respect to the blank solution, signaling the initiation of inhibition. This implies that **AEPA** starts to accumulate on the metallic surface, thereby creating a protective layer.[70] On increasing the concentration to 5–10 mM, the capacitive loop increased further, indicating enhanced surface coverage and improved protection effects. The parameters listed in Table 3 indicate a remarkable increase in R_{ct} from 171.62 Ω cm^2 at 1 mM to 387.55 Ω cm^2 at 10 mM. The trend agrees with the progressive formation of a denser and more protective layer at increasing inhibitor concentration.[71] The same trends were found for **DOCA** (Fig. 7b): at the concentration of 1 mM, the Nyquist plot (Fig. 7b) revealed the initial rise in the diameter of the capacitive loop, revealing the onset of inhibition. Raising the concentration to 5–10 mM **DOCA** led to a further widening of the capacitive loop, in accordance with a higher surface coverage. Fitted parameters in Table 3 reveal a significant rise in R_{ct} from 138.93 Ω cm^2 at 1 mM to 345.80 Ω cm^2 at 10 mM, providing the increased protective function of **DOCA** at higher concentrations.[72] The Bode phase angle and modulus plots (Fig. 7c and d) give further information on the impedance behavior. In the absence of any inhibitor, the Bode modulus plot reveals a significant reduction in impedance magnitude at lower frequencies, revealing a quick charge transfer through the metal/solution interface. Conversely, the phase angle plot displays a steep decline, revealing the highly capacitive nature of the system.[73,74] Addition of **AEPA** and **DOCA** provides Bode modulus plots that exhibit an increase in impedance values throughout the whole frequency range, more so at low frequencies.[55] The observation indicates that the inhibitors oppose charge transfer mechanisms and lead to a decrease in the overall corrosion rate.[75] The phase angle plots also depict a more negative values, corresponding to a shift towards more resistive behavior, typical of good corrosion inhibition.[76,77] The EIS data were analyzed using an equivalent circuit model composed of solution resistance (R_s), charge transfer resistance (R_{ct}), film formation resistance (R_f), and constant phase elements (CPEs) for the double-layer capacitance and the adsorbed inhibitor film. The fitting parameters are given in Table 3. For **AEPA**, R_{ct} increased from 171.62 Ω cm^2 at 1 mM to 387.55 Ω cm^2 at 10 mM. For **DOCA**, R_{ct}

increased from 138.93 Ω cm^2 at 1 mM to 345.80 Ω cm^2 at 10 mM. These improvements in R_{ct} demonstrate a direct correlation with the formation of a protective film on the metallic surface, thus effectively preventing electron transfer processes.[78] Both the **AEPA** and **DOCA** both showed a decrease in C_{dl}. The increase in concentration implies the formation of a dense and small-sized protective layer, which reduces the surface area available for charge transfer.[79] Surface coverage (θ) also increased with inhibitor concentration to attain maximum values of 0.9554 for **AEPA** and 0.9499 for **DOCA** at 10 mM. Such high surface coverage agrees with inhibition efficiencies greater than 94%, which obviously reflects the high adsorption capacity of both compounds.[80] The inhibition efficiencies calculated from EIS data (η_z) exceeded 94% at 10 mM for **AEPA** and **DOCA**. The rise in R_{ct} and R_f and the decrease in C_{dl} and C_f suggest that both compounds adsorb onto the surface of the carbon steel to form a protective film, which inhibits ingress of corrosive species (*e.g.*, H^+) to the metal.[81] The structural features of **AEPA** and **DOCA**, such as the nitrogen and sulfur atoms, are likely to interact with iron atoms at the metallic surface, thus enhancing the strength and stability of adsorption.[82]

3.3. Adsorption isotherm

To gain further insight into the interaction of **AEPA** and **DOCA** molecules with the carbon steel surface in 1.0 M HCl solution, adsorption isotherm studies were conducted based on electrochemical data. These studies are extremely valuable in furnishing details about the nature and strength of inhibitor adsorption and hence corrosion inhibition efficiency.[83,84] Besides the Langmuir model, the adsorption data were also analyzed using various isotherm models such as Freundlich, Frumkin, Temkin, Flory–Huggins, and kinetic-thermodynamic models. The results are represented in Fig. 8 and Table 4. From linear regression analysis, high correlation coefficients ($R^2 > 0.99$, closet to ≈ 1), indicating that the Langmuir model best describes the adsorption process.[85] This model considers monolayer coverage without any lateral interaction between the adsorbed molecules and is mathematically expressed as:[86,87]

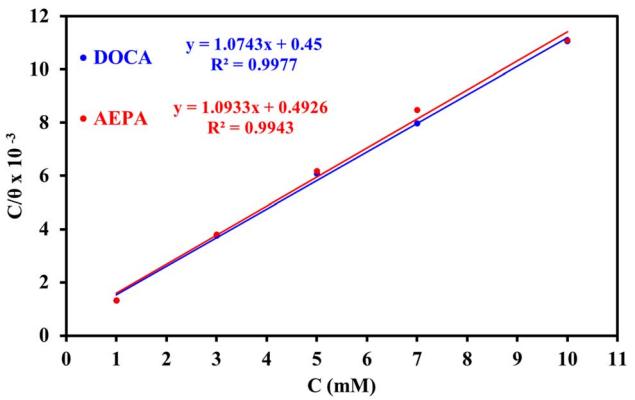

Fig. 8 The Langmuir adsorption model for AEPA and DOCA compounds on the steel surface in 1.0 M HCl using data obtained from PDP measurements at 30 °C.

$$\frac{C}{\theta} = \frac{1}{K_{ads}} + C \quad (4)$$

where C is the inhibitor concentration, θ is the surface coverage, and K_{ads} is adsorptive capacity is directly connected with the equilibrium constant. Fig. 8 shows the Langmuir plots for both inhibitors at 30 °C. From these plots, the values of K_{ads} and the standard Gibbs free energy of adsorption (ΔG_{ads}) were calculated[88] and are given in Table 4.

$$\Delta G_{ads} = -RT \ln 55.5\ K_{ads} \quad (5)$$

The calculated K_{ads} values were 2222 M^{-1} for **AEPA** and 2030 M^{-1} for **DOCA**. These values indicate enhanced adsorption affinity among the inhibitor molecules and the metal surface.[89] The calculated ΔG_{ads} values were −29.53 kJ mol^{-1} for **AEPA** and −29.30 kJ mol^{-1} for **DOCA**. The values obtained confirm that the adsorption mechanism is spontaneous and exothermic in nature.[90] Values between −20 and −40 kJ mol^{-1} are normally representative of a mixture of physisorption and chemisorption;[91] however, the appreciable magnitude in this case points towards a predominance of chemisorption. The presence of lone-pair electrons in nitrogen and sulfur atoms enables the atoms to donate electron density to empty d-orbitals of iron, thereby creating stable chemical bonds and increasing surface protection.[92]

For Freundlich model that accounts for heterogeneous surfaces and multilayer adsorption, the slopes ($1/n$) were found to be less than 1, indicating good conditions for adsorption. Specifically, $1/n = 0.07729$ for **AEPA** and $1/n = 0.06695$ for **DOCA**, indicating moderate heterogeneity and easiness of the adsorption process.[93] The Frumkin model incorporates interactions between adsorbed species. The slopes' negative values (−2.99560 for **AEPA** and −3.10908 for **DOCA**) indicate repulsive interactions between adsorbed species, as is typical for organic corrosion inhibitors.[94]

3.4. FE-SEM/EDX analysis

For 24 hours, carbon steel samples were immersed in 1.0 M hydrochloric acid and examined using a scanning electron microscope (SEM). This analysis was carried out on polished samples treated with **DOCA** and **AEPA** inhibitors. Fig. 9a shows the polished carbon steel before exposure to the corrosive acid. Removing rust with silica carbide plates damages the surface of the carbon steel, causing inevitable roughening. Fig. 9b shows an SEM image of the metal and carbon surface in 1.0 M hydrochloric acid. Without an inhibitor, the corrosion damages the surface. The carbon steel surface exposed to acid corrosion displays several visible voids of different sizes and depths, indicating significant material loss. The corrosive liquid dissolves the surface, making it rough. A dense, porous layer of corrosion residues, including oxide coatings, covers the metal surface and causes damage.[95] Adding 10 mM **DOCA** and **AEPA** to the corrosive solution, as shown in Fig. 10a and b, significantly reduced damage to the sample surface. Pits and cracks were less severe than those in Fig. 9b. SEM images of carbon steel in 1.0 mM hydrochloric acid with 10 mM **DOCA** showed numerous

Table 4 Adsorption isotherms models of the inhibitors with values of R^2, slopes, intercepts, K_{ads}, and ΔG_{ads} obtained by using data from electrochemical measurements[a]

Adsorption isotherm model	Linear form equation	Technique	Inhibitor	Slope	Intercept	R^2	K_{ads} M^{-1}	ΔG_{ads} kJ mol^{-1}
Freundlich	$\log\theta = \log K + 1/n \log C$	PDP	**AEPA**	0.07729	0.10450	0.92991	1.2720	−10.72
			DOCA	0.06695	0.07110	0.82530	1.1779	−10.53
Langmuir	$\frac{c}{\theta} = \frac{1}{K} + c$	EFM	**AEPA**	1.04959	0.00032	0.99865	3107	−30.38
			DOCA	1.06109	0.00035	0.99749	2831	−30.14
		EIS	**AEPA**	1.03773	0.00013	0.99989	7952	−32.74
			DOCA	1.04134	0.00013	0.99996	7534	−32.61
		PDP	**AEPA**	1.07433	0.00045	0.99773	2222	−29.53
			DOCA	1.09335	0.00049	0.99428	2030	−29.30
Frumkin	$\log\frac{\theta}{(1-\theta)C} = \log K + 2a\theta$	PDP	**AEPA**	−2.99560	5.60703	0.65745	4.0460×10^5	−42.64
			DOCA	−3.10908	5.59530	0.43833	3.9382×10^5	−42.57
Temkin	$\theta = -\frac{1}{2a}\ln C - \frac{1}{2a}\ln K$	PDP	**AEPA**	14.40442	−17.50380	0.91747	0.2967	−7.06
			DOCA	14.66604	−17.47807	0.80223	0.3037	−7.12
Flory–Huggins	$\log\left(\frac{\theta}{c}\right) = \log K + n\log(1-\theta)$	PDP	**AEPA**	1.99024	3.90529	0.82977	8.0406×10^3	−32.77
			DOCA	1.94352	3.77006	0.65370	5.8893×10^3	−31.99
Kinetic-thermodynamic	$\log\left(\frac{\theta}{1-\theta}\right) = \log K + y\log c$	PDP	**AEPA**	0.46591	1.83453	0.86205	8660.764	−32.96
			DOCA	0.38832	1.59409	0.70887	39.2727	−19.36

[a] R^2 = regression correlation coefficient, K = binding constant, θ = surface coverage, c = concentration.

areas with smoother surfaces and fewer cracks. **AEPA** appears to form a protective layer on the carbon steel, unlike the uniform **DOCA** inhibitor, which directly adheres to the metal surface.[96] **DOCA** and **AEPA** protect metal surfaces from corrosion in 1.0 mM hydrochloric acid by forming a barrier. They improve the steel's surface and prevent contact with the corrosive solution, halting corrosion. According to EDX analysis, **DOCA** contains a small amount of nitrogen by weight and 0.2% sulfur. The **AEPA** inhibitor contains 71.4% iron, while the **DOCA** inhibitor contains 71.5% iron, along with some additional elements.

Based on these findings, it appears that carbon steel can naturally develop protective layers. The EDX mapping images illustrate the spatial arrangement of the elements, as shown in Fig. 10a and b. By incorporating and displaying nitrogen, sulfur, and oxygen atoms on the steel's surface, the inhibitors' composition prevents corrosion.[97]

3.5. Theoretical calculations

3.5.1. Optimization and frontier molecular orbital analysis (FMOs). The compounds were first optimized, as shown in Fig. 11. Based on the FMO theory, we hypothesized that the corrosion inhibition efficiency could be assessed through an analysis of their electronic properties. Energy of HOMO demonstrate molecule's tendency to donate electrons, while the energy of LUMO displays its capability to accept electrons. A good corrosion inhibitor typically demonstrates the higher HOMO energy and a lower LUMO energy. The higher HOMO energy indicates a better tendency to donate electrons to metal surface, which eases the formation of a shielding layer.[98,99] A lower LUMO energy shows a reduced tendency of the inhibitor to accept electrons from metal surface, which helps in suppressing the corrosion process. So, an inhibitor with a higher energy gap is typically considered more efficient in preventing corrosion.[100,101] The computed HOMO values for **AEPA** and **DOCA** are −5.65 eV and −6.70 eV, respectively (see Fig. 12). **AEPA** exhibits a higher HOMO energy compared to **DOCA**. As shown in Fig. 2, **AEPA** has a LUMO energy of −1.12 eV, while **DOCA** has a LUMO energy of −0.85 eV. This suggests that **AEPA** has lower LUMO.

Lowering the energy gap between the HOMO and LUMO (ΔE) is crucial to improving the efficiency of the corrosion inhibitions of these compounds. The lower the ΔE, the easier is electron transfer, which is important for the formation of protective films on a metal surface.[102,103] As shown in Fig. 12, **AEPA** is with energy gap of 4.53 eV where as **DOCA** is with energy gap of 5.85 eV. This means that **AEPA** possess a lower ΔE, which is indicative of a greater potential to adsorb onto the metal surface, owing to its better electron transfer ability.[104,105] The FMO results are confirmed by the DOS results as well (see Fig. 13). DOS is a measure of the available electronic states within a specific energy range.[106,107] It is useful in understanding contributions of molecular fragments to molecular orbitals and can be estimated by the distribution of states in energy. Examinations in terms of the FMOs, their compositions and the DOS near HOMO and LUMO levels reveal that the variation of

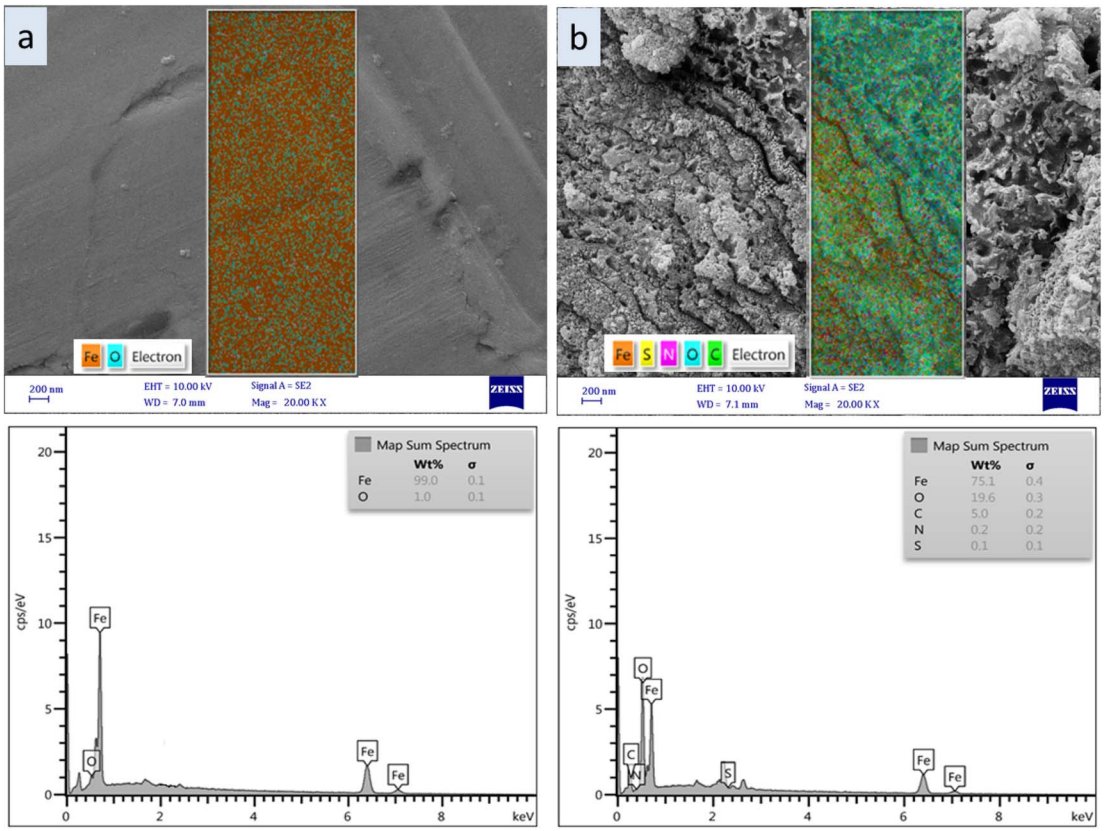

Fig. 9 SEM and EDX images of the steel surface (a) polished and (b) after 24 hours immersion in 1.0 M HCl.

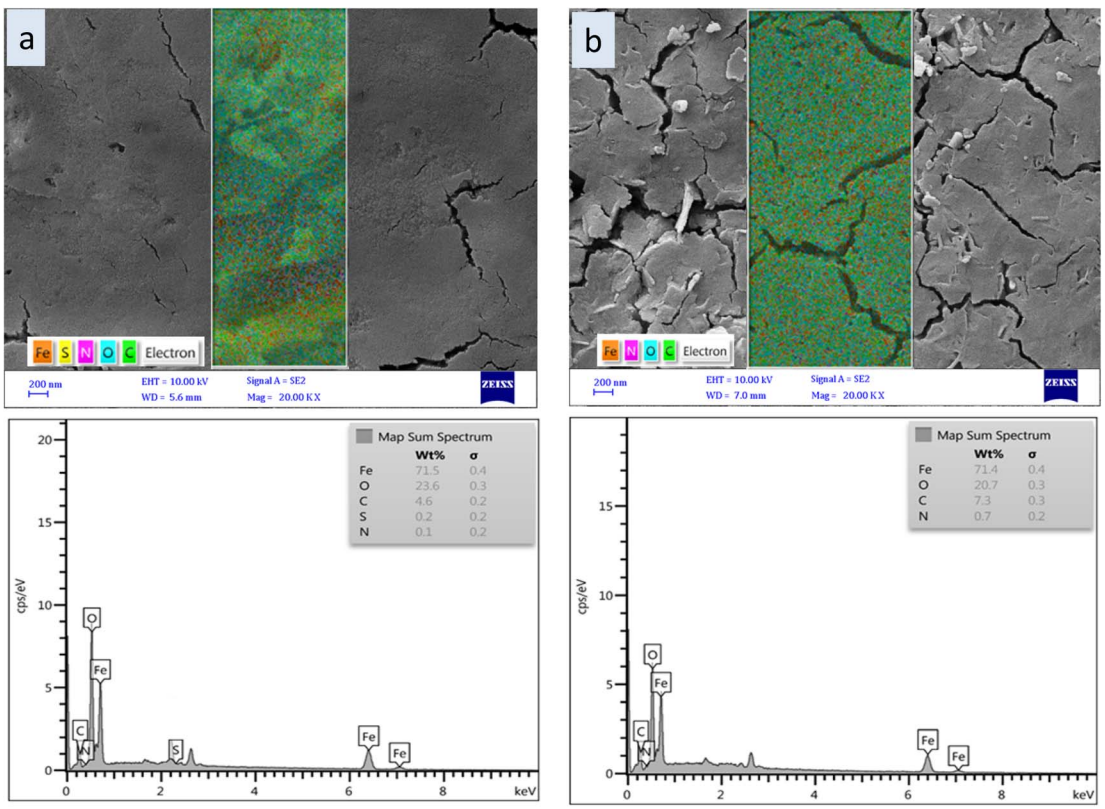

Fig. 10 SEM and EDX images of the steel surface after 24 hours immersion in 1.0 M HCl containing 10 mM of **AEPA** (a) and **DOCA** (b).

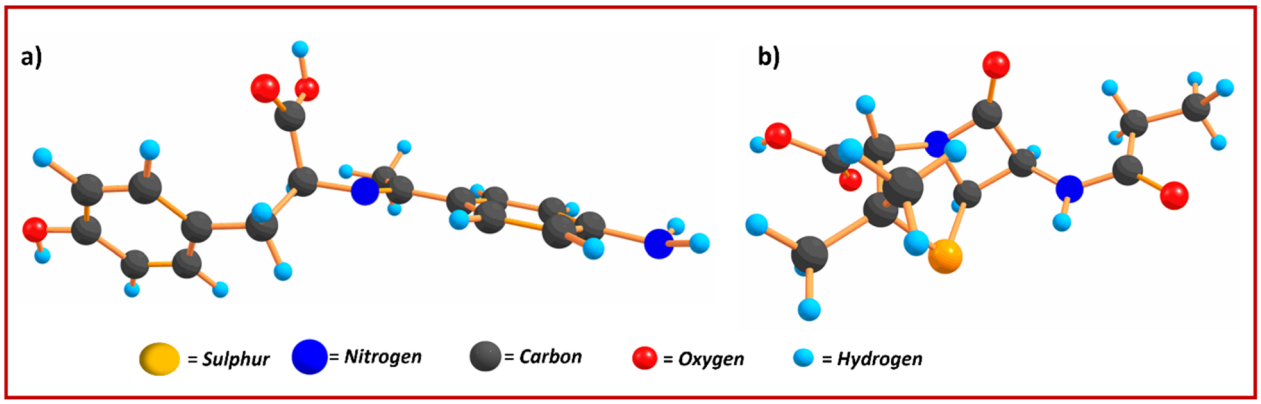

Fig. 11 Optimized structures of AEPA (a) and DOCA (b).

electron-withdrawing abilities of the acceptor groups mainly influences the electron densities in the orbitals. In the DOS map, positive energy represents the bonding orbitals, negative energy is represented by antibonding states, and zero by no bond interaction states. The DOS results are consistent with the FMO analysis. Thus, DOS spectra can be used as a quantitative

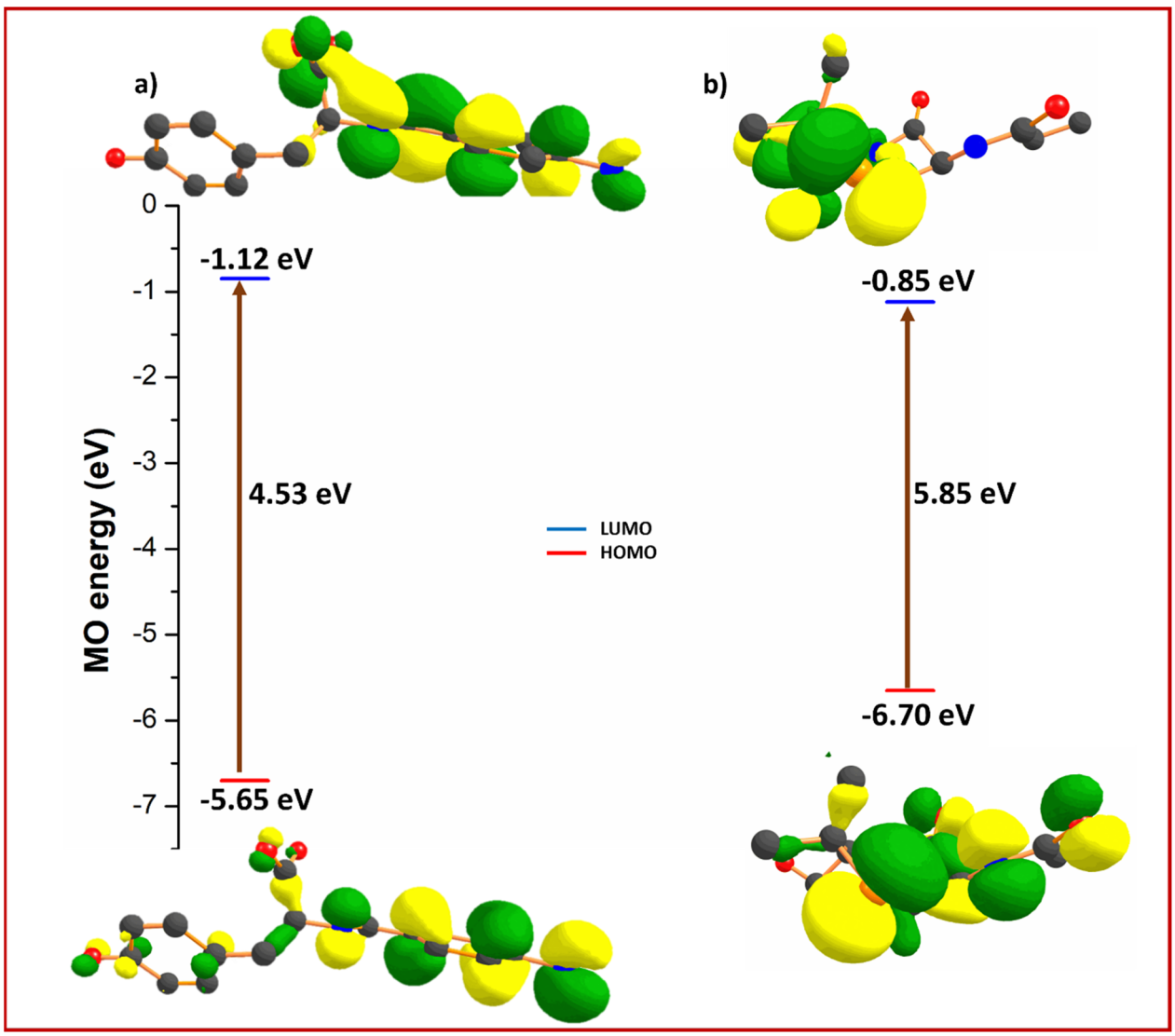

Fig. 12 Frontier molecular orbitals and energy gap of AEPA (a) and DOCA (b).

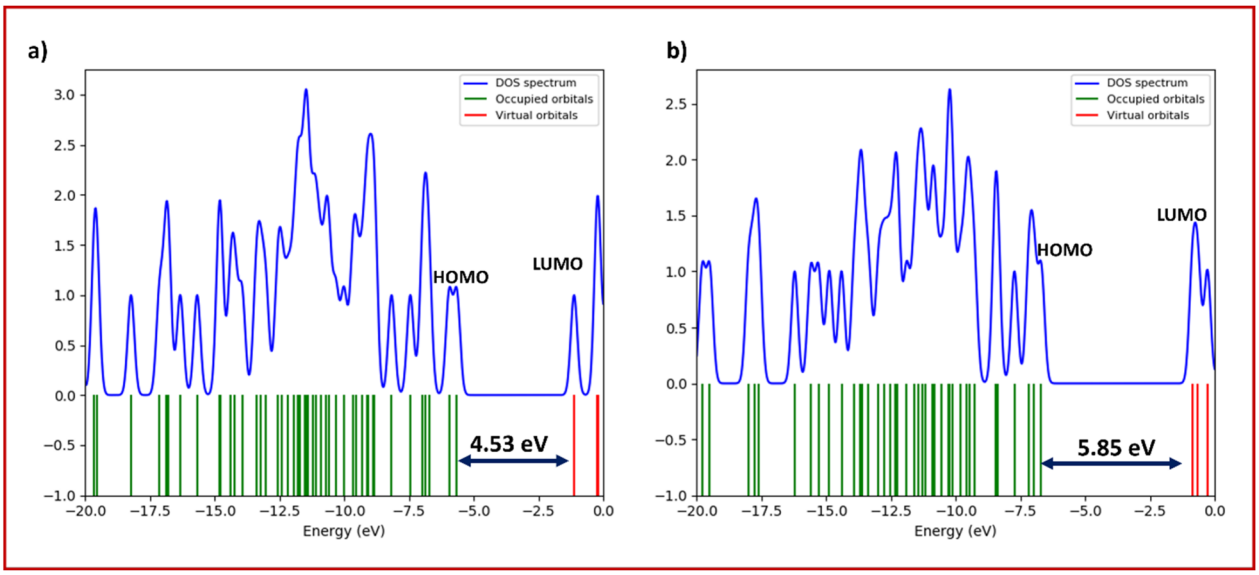

Fig. 13 Density of states of compounds AEPA (a) and DOCA (b).

tool to study electronic interactions in the system. Furthermore, the FMOs are used to calculate the global reactivity descriptors, which contribute to understand the chemical reactivity of **AEPA** and **DOCA**. These descriptors serve to relate energy levels, molecular structure, and reactivity and include ionization potential, electron affinity, electronegativity, chemical hardness, softness, and dipole moment (μ) among the parameters. These descriptors have been obtained from the Koopmans' theorem (see Table 5).[108] Generally, the lower value of electronegativity means that the inhibitor has a high tendency to give electrons to the metal surface. Conversely, molecules with higher electronegativity are more susceptible to accept electrons from the steel surface (back-donation) and develop a stronger interaction with the metal. It can be seen from Table 5 that **AEPA** and **DOCA** show a higher electronegativity, which tends to back-donate and lead to strong adsorption at the metal interface. Similarly, the softness (S) and hardness (η) are important parameters to estimate the stability and reactivity of inhibitor molecules. Soft molecules are better corrosion inhibitors than hard molecules because of their higher degree of electron transfer to the metal surface upon adsorption.[109] It can be seen from Table 5 that **AEPA** has a higher inhibition efficiency compared with **DOCA** due to its low softness and high hardness values. The electron-donating and accepting tendencies of the inhibitor are further evaluated through the concept of back-donation. A negative ΔE back-donation value indicates that the molecule extracts electrons from metal surface atoms. Sequentially, electron-deficient metal atoms attempt to regain electrons from the molecule *via* back-donation. This reciprocal electron exchange is dynamically favourable and strengthens

Table 5 The calculated global reactivity indices of AEPA and DOCA inhibitors in different medium[a]

	AEPA		**DOCA**	
Molecular parameters	Gas phase	Aqueous	Gas phase	Aqueous
E_{LUMO}	−1.12	−0.376	−0.85	−1.079
E_{HOMO}	−5.65	−5.514	−6.7	−6.365
ΔE	4.53	5.139	5.85	5.287
Ionization potential (I)	5.65	5.514	6.7	6.365
Electron affinity (A)	1.12	0.376	0.85	1.079
Electronegativity (χ)	3.385	2.945	3.775	3.722
Chemical potential (μ)	−3.385	−2.945	−3.775	−3.722
Chemical hardness (η)	2.265	2.569	2.925	2.643
Chemical softness (σ)	0.442	0.389	0.342	0.378
Global electrophilicity index (ω)	2.529	1.688	2.436	2.62
Fraction of electron transferred (ΔN)	1.35	1.276	0.979	1.093
μ (debye)	4.74	19.4	5.00	8.09

[a] IP (Ionization Potential) $= -E_{HOMO}$, EA (Electron Affinity) $= -E_{LUMO}$, hardness$(\eta) = \frac{(IP - EA)}{2}$, softness$(S) = \frac{1}{\eta}$, electronegativity$(\chi) = \frac{(IP + EA)}{2}$, $\Delta E_{back\text{-}donation} = \frac{-\eta}{4}$.

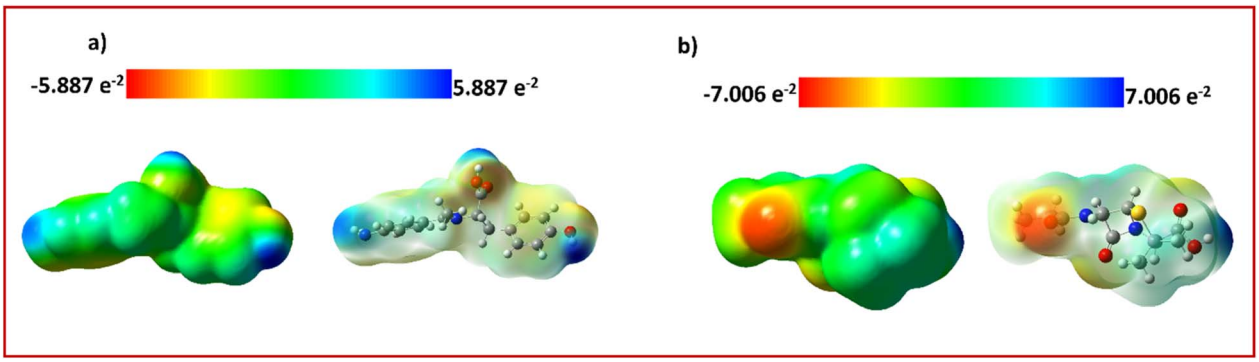

Fig. 14 MEP maps of compounds **AEPA** (a) and **DOCA** (b).

the interaction between inhibitor and metal surface. Table 5 shows that **AEPA** and **DOCA** exhibit negative ΔE back-donation values, signifying that back-donation is a favourable mechanism contributing to strong bonding at the metal interface.[110] The μ is an additional significant factor in assessing corrosion inhibition performance. A higher dipole moment characteristically enhances the molecule's capability to adsorb onto the metal surface and upsurges the associated distortion energy. Thus, greater dipole moments are often linked to more effective corrosion protection. According to Table 5, **DOCA** exhibits a notably higher dipole moment (5.00 debye) than **AEPA** (4.74 debye), signifying a stronger tendency for adsorption onto the metal surface and, possibly, better inhibition efficiency.

3.5.2. Molecular electrostatic potential (MEP). MEP maps are valuable tools for classifying the reactive regions within a molecule, highlighting the possible sites for electrophilic and nucleophilic attacks. MEP maps show the interaction energy between a molecule's electron distribution and a hypothetical positive test charge. The colour gradient ranges from red, blue, to green, demonstrating regions of negative, positive, and neutral potential, respectively. Red areas denote regions with strong nucleophilic character, making them favourable for electrophilic attack, whereas dark blue areas suggest an electrophilic nature, possible to attract nucleophiles. Yellow and light blue areas specify less intense nucleophilic and electrophilic regions, respectively, and green signifies zones of neutral electrostatic potential.[111–120] For **AEPA**, a red zone seems around the O_2 atom, blue over the hydroxyl hydrogen, and green spreads over the whole (4-aminophenyl ethylidene amino-3-hydroxypropyl)phenol moiety. Likewise, **DOCA** shows a red region near the O_2 atom, a blue region over the hydroxyl hydrogen, and a green area extending across the trimethyl-*N*-propyl-4-thia-1-azabicyclo[3.2.0]heptan-6-amine group. The electrostatic potential values for **AEPA** and **DOCA** are -5.887×10^{-2} and -7.006×10^{-2}, respectively. These results, as shown in Fig. 14, specify that **DOCA** possesses a more electronegative surface potential than **AEPA**.

4. Conclusion

The current research illustrates that the prepared **AEPA** and **DOCA**, are highly efficient corrosion inhibitors for carbon steel in exposure to 1.0 M HCl solution. The following conclusions can be drawn:

Electrochemical measurements (PDP, EFM, and EIS) revealed that both compounds effectively reduce the corrosion current density, with the highest inhibition efficiencies above 93% at 10 mM concentration. Adsorption studies showed that the inhibitors follow the Langmuir isotherm, indicating monolayer formation through chemisorption by nitrogen and sulfur donor atoms. Thermodynamic factors like the standard Gibbs free energy change (ΔG^0_{ads}) favored both the spontaneity and exothermicity of the adsorption process. Both of the compounds exhibited a mixed-type inhibition profile, effectively blocking both anodic and cathodic processes.

The analysis of **AEPA** and **DOCA**, based on Frontier Molecular Orbital (FMO) theory and Density of States (DOS) analysis, revealed that **AEPA** exhibits better corrosion inhibition properties due to its smaller HOMO–LUMO energy gap, higher HOMO energy, and lower LUMO energy compared to **DOCA**. These properties suggest that **AEPA** has a greater propensity for electron donation, facilitating its adsorption onto metal surfaces and forming protective layers that inhibit corrosion. Additionally, **AEPA**'s lower softness and higher hardness further enhance its stability and reactivity as a corrosion inhibitor. While **DOCA** exhibits a higher dipole moment, suggesting strong adsorption potential, **AEPA** demonstrates overall superior performance in preventing corrosion. The global reactivity descriptors and MEP analysis reinforce these findings, indicating that **AEPA** is more effective in protecting metal surfaces against corrosion due to its favorable electronic properties and molecular structure.

Conflicts of interest

The authors declare that they have no known competing financial interests or personal relationships that could have appeared to influence the work reported in this paper.

Data availability

The data supporting the findings of this study are available within the article. Additional data can be provided by the corresponding author upon reasonable request.

Acknowledgements

During the preparation of this work the author(s) used QUILBOT to improve readability and language of the work. After using this tool/service, the author(s) reviewed and edited the content as needed and took(s) full responsibility for the content of the publication. The authors are thankful to the Deanship of Graduate Studies and Scientific Research at University of Bisha for supporting this work through the Fast-Track Research Support Program. This work was also supported by the Deanship of Scientific Research, Vice Presidency for Graduate Studies and Scientific Research, King Faisal University, Saudi Arabia [Grant No. KFU252548].

References

1 M. M. Y. Modwi, H. Feng, M. K. Hadi, N. Chen, J. Hou, E. Kamal and K. Yang, Eco-friendly corrosion inhibitor of Q235 carbon steel in 1.0 M HCl by Isatin/Chitosan Schiff base, *J. Mol. Struct.*, 2025, **1321**, 139592, DOI: 10.1016/j.molstruc.2024.139592.

2 Q. A. Yousif, S. S. Malhotra, M. A. Bedair, A. Ansari and A. K. Hadi, Safflower plant extract as a sustainable corrosion inhibitor for carbon steel in acidic media: a combined electrochemical and computational study, *RSC Adv.*, 2025, **15**, 21006–21025, DOI: 10.1039/D5RA03333K.

3 F. Kaya, R. Solmaz and İ. H. Geçibesler, Adsorption and corrosion inhibition capability of Rheum ribes root extract (Işgın) for mild steel protection in acidic medium: A comprehensive electrochemical, surface characterization, synergistic inhibition effect, and stability study, *J. Mol. Liq.*, 2023, **372**, 121219, DOI: 10.1016/j.molliq.2023.121219.

4 Q. A. Yousif, M. Ranjeh, M. Ghiyasiyan-Arani, A. Al-Nayili, R. Monsef and M. Salavati-Niasari, Morphology engineering of LiFeO2 nanostructures through synthesis controlling for electrochemical hydrogen storage inquiries, *Fuel*, 2022, **313**, 123025, DOI: 10.1016/j.fuel.2021.123025.

5 P. D. Desai, C. B. Pawar, M. S. Avhad and A. P. More, Corrosion inhibitors for carbon steel: A review, *Vietnam J. Chem.*, 2023, **61**, 15–42, DOI: 10.1002/vjch.202200111.

6 Z. Fadel and Q. A. Yousif, Inhibitory action of a new derivative of amino acids in aerated acidic media, *IOP Conf. Ser.: Earth Environ. Sci.*, 2021, **790**, 012074, DOI: 10.1088/1755-1315/790/1/012074.

7 A. Royani, M. Hanafi, R. Haldhar and A. Manaf, Evaluation of Morinda citrifolia extract as sustainable inhibitor for mild steel in saline environment, *J. Eng. Res.*, 2024, 1–7, DOI: 10.1016/j.jer.2024.01.013.

8 M. N. Majeed, Q. A. Yousif and M. A. Bedair, Study of the Corrosion of Nickel–Chromium Alloy in an Acidic Solution Protected by Nickel Nanoparticles, *ACS Omega*, 2022, **7**, 29850–29857, DOI: 10.1021/acsomega.2c02679.

9 E. H. Alosaimi, Some prepared schiff-base complexes for corrosion inhibition of steel in hydrochloric acid solution, *Mater. Chem. Phys.*, 2025, **333**, 130332, DOI: 10.1016/j.matchemphys.2024.130332.

10 M. H. Rahmani, A. Dehghani, M. Salamati, G. Bahlakeh and B. Ramezanzadeh, Mango extract behavior as a potent corrosion inhibitor against simulated chloride-contaminated concrete pore solution; coupled experimental and computer modeling studies, *J. Ind. Eng. Chem.*, 2024, **130**, 368–381, DOI: 10.1016/j.jiec.2023.09.040.

11 M. A. Bedair, A. M. Abuelela, S. Melhi, Q. A. Yousif, V. V. Chaban and E. H. Alosaimi, Highly effective inhibition of steel corrosion in 1.0 M HCl solution using a novel non-ionic surfactant with coumarin moiety: Practical and computational studies, *Mater. Chem. Phys.*, 2024, **312**, 128644, DOI: 10.1016/j.matchemphys.2023.128644.

12 R. Lei, S. Deng, Y. Qiang, D. Xu, G. Du, D. Shao and X. Li, Sunflower stalk extract as a novel green inhibitor on aluminium corrosion in HCl solution, *Colloids Surf., A*, 2024, **687**, 133358, DOI: 10.1016/j.colsurfa.2024.133358.

13 M. S. Mohamad Sidik, M. H. Abu Bakar and H. Allal, Adsorption of Benzene-1,4-diol, 3-Methyl-1,2-cyclopentanedione and 2,6-Dimethoxyphenol on aluminium (1 1 1) plane using density functional theory calculations, *Chem. Phys.*, 2022, **560**, 111592, DOI: 10.1016/j.chemphys.2022.111592.

14 Q. A. Yousif, Z. Fadel, A. M. Abuelela, E. H. Alosaimi, S. Melhi and M. A. Bedair, Insight into the corrosion mitigation performance of three novel benzimidazole derivatives of amino acids for carbon steel (X56) in 1 M HCl solution, *RSC Adv.*, 2023, **13**, 13094–13119, DOI: 10.1039/D3RA01837G.

15 Q. A. Yousif, M. A. Bedair, A. M. Abuelela, F. Al-odail, A. Ansari and Z. Fadel, Theoretical and experimental aspects of novel penicillanic acid compounds as corrosion inhibitors in acidic solutions, *Mater. Today Commun.*, 2025, **47**, 113199, DOI: 10.1016/j.mtcomm.2025.113199.

16 H. M. Abd El-Lateef, W. M. Abd El-Monem Nasr, M. M. Khalaf, A. E. Mohamed, M. N. Rashed and M. S. S. Adam, Anticorrosion Evaluation of Novel Water-Soluble Schiff Base Molecules for C1018 Steel in CO2-Saturated Brine by Computational and Experimental Methodologies, *ACS Omega*, 2023, **8**, 11512–11535, DOI: 10.1021/acsomega.3c00561.

17 E. H. Haasan and Q. A. Yousif, Synthesis and characterization of new PTh- MMT and PTh @ MMT-CuSO 4 nanocomposites Synthesis and Characterization of New PTh-MMT, *AIP Conf. Proc.*, 2023, **2414**, 050040, DOI: 10.1063/5.0114733.

18 M. Galai, K. Dahmani, O. Kharbouch, M. Rbaa, N. Alzeqri, L. Guo, A. A. AlObaid, A. Hmada, N. Dkhireche, E. Ech-chihbi, M. Ouakki, M. E. Touhami and I. Warad, Surface analysis and interface properties of a newly synthesized quinoline-derivative corrosion inhibitor for mild steel in acid pickling bath: Mechanistic exploration through electrochemical, XPS, AFM, contact angle, SEM/EDS, and computational studies, *J. Phys. Chem. Solids*, 2024, **184**, 111681, DOI: 10.1016/j.jpcs.2023.111681.

19 Z. Fadel and Q. A. Yousif, (2S,3R)-2-((1-(4-amionophenyl) ethylidene)amino)-3-hydroxybutanoic acid as a novel and eco-friendly corrosion inhibitor for the carbon steel (X56) used in Iraq's oil installations, *J. Phys.: Conf. Ser.*, 2020, **1664**, 012093, DOI: 10.1088/1742-6596/1664/1/012093.

20 Z. Zhang, P. Gan, D. Zhang and L. Gao, Corrosion inhibition of 8-HQ for AA5052 in 3 wt% NaCl solution in presence of trace Cu2+ ions: Electrochemical/surface studies, DFT/MD modeling, *Desalin. Water Treat.*, 2024, **317**, 100143, DOI: 10.1016/j.dwt.2024.100143.

21 W. J. Long, X. Q. Li, S. Y. Zheng and C. He, A novel effective carbon dots-based inhibitor for carbon steel against chloride corrosion: From inhibition behavior to mechanism, *Carbon*, 2024, **218**, 118708, DOI: 10.1016/j.carbon.2023.118708.

22 Q. A. Yousif, A. Abdel Nazeer, Z. Fadel, L. A. Al-Hajji and K. Shalabi, Design of New Ecofriendly Schiff Base Inhibitors for Carbon Steel Corrosion Protection in Acidic Solutions: Electrochemical, Surface, and Theoretical Studies, *ACS Omega*, 2024, **9**, 14153–14173, DOI: 10.1021/acsomega.3c09688.

23 M. Valian, F. Soofivand, A. Khoobi, Q. A. Yousif and M. Salavati-Niasari, A Green Approach: Eco-friendly Synthesis of Gd2Ti2O7/N-GQD Nanocomposite and Photo-Degradation and Electrochemical Measurement of Hydroxychloroquine as a Perdurable Drug, *Arabian J. Chem.*, 2022, **16**, 104401, DOI: 10.1016/j.arabjc.2022.104401.

24 Z. Sabet-Bokati, K. Sabet-Bokati, Z. Russell, K. Morshed-Behbahani and S. Ouanani, Anticorrosion shape memory-assisted self-healing coatings: A review, *Prog. Org. Coat.*, 2024, **188**, 108193, DOI: 10.1016/j.porgcoat.2023.108193.

25 M. S. Mohamad Sidik, M. H. Abu Bakar and H. Allal, Adsorption of Benzene-1,4-diol, 3-Methyl-1,2-cyclopentanedione and 2,6-Dimethoxyphenol on aluminium (1 1 1) plane using density functional theory calculations, *Chem. Phys.*, 2022, **560**, 111592, DOI: 10.1016/j.chemphys.2022.111592.

26 X. Wang, H. Guo, S. Cai and X. Xu, Expired antihypertensive drugs as eco-friendly and efficient corrosion inhibitors for carbon steel in CO2-saturated oilfield water: Experimental and theoretical approaches, *J. Mol. Struct.*, 2023, **1294**, 136555, DOI: 10.1016/j.molstruc.2023.136555.

27 N. Xu, X. B. Yang and Q. H. Zhang, Insight into interfacial adsorption and inhibition mechanism of Aconitum carmichaelii Debx extract as high-efficient corrosion inhibitor for carbon steel in acidic solution, *J. Mol. Liq.*, 2024, **393**, 123602, DOI: 10.1016/j.molliq.2023.123602.

28 M. Naciri, S. Skal, Y. El Aoufir, M. R. Al-hadeethi, H. Lgaz, H. Bidi, M. El Moudane, A. Ghanimi and A. Bellaouchou, Unveiling the influence of furan and thiophene on the corrosion inhibition capabilities of novel hydrazones derivatives in carbon steel/HCl interface: A dual experimental-theoretical study, *Colloids Surf., A*, 2024, **686**, 133272, DOI: 10.1016/j.colsurfa.2024.133272.

29 P. R. R. Sagunthala Devi, S. T. David, C. Joel, R. B. Bennie and S. D. Abraham, Studies on corrosion inhibition efficiencies of new mixed ligand complexes of SNSN donor Schiff base and NN donor 2-2′-bipyridine with 3d metal ions, *Mater. Chem. Phys.*, 2025, **332**, 130279, DOI: 10.1016/j.matchemphys.2024.130279.

30 L. Kaghazchi, R. Naderi and B. Ramezanzadeh, Improvement of the dual barrier/active corrosion inhibition function of the epoxy composite filled with zinc doped-phytic acid-modified graphene oxide nanosheets, *Prog. Org. Coat.*, 2022, **168**, 106884, DOI: 10.1016/j.porgcoat.2022.106884.

31 L. Huang, S. S. Wang, H. J. Li, J. Y. Wang, Z. G. Li and Y. C. Wu, Highly effective Q235 steel corrosion inhibition in 1 M HCl solution by novel green strictosamide from Uncaria laevigata: Experimental and theoretical approaches, *J. Environ. Chem. Eng.*, 2022, **10**, 107581, DOI: 10.1016/j.jece.2022.107581.

32 M. Lavanya and A. A. Machado, Surfactants as biodegradable sustainable inhibitors for corrosion control in diverse media and conditions: A comprehensive review, *Sci. Total Environ.*, 2024, **908**, 168407, DOI: 10.1016/j.scitotenv.2023.168407.

33 C. Tio, Q. A. Yousif, N. Majeed and M. A. Bedair, Surface protection against corrosion of Ni turbine, *RSC Adv.*, 2022, 33725–33736, DOI: 10.1039/D2RA06949K.

34 Q. A. Yousif, M. A. Bedair, Z. Fadel, F. Al-Odail and A. M. Abuelela, Evaluating the efficacy of newly synthesized amino acid derivatives as corrosion inhibitors in acidic solutions, *Inorg. Chem. Commun.*, 2024, **164**, 112454, DOI: 10.1016/j.inoche.2024.112454.

35 J. Supardi, S. Rizal, N. Ali, S. Fonna, I. Ikramullah and A. K. Arifin, Investigating an environmentally in aqueous solution of potacium chloride, *J. Mater. Res. Technol.*, 2024, **29**, 303–310, DOI: 10.1016/j.jmrt.2024.01.137.

36 X. Ding, L. Zhao, I. M. Khan, L. Yue, Y. Zhang and Z. Wang, Emerging chitosan grafted essential oil components: A review on synthesis, characterization, and potential application, *Carbohydr. Polym.*, 2022, **297**, 120011, DOI: 10.1016/j.carbpol.2022.120011.

37 Q. A. Yousif, M. A. Bedair, A. M. Abuelela, F. Al-Odail, A. Ansari and Z. Fadel, Theoretical and experimental aspects of novel penicillanic acid compounds as corrosion inhibitors in acidic solutions, *Mater. Today Commun.*, 2025, **47**, 113199, DOI: 10.1016/j.mtcomm.2025.113199.

38 M. A. Bedair, Q. A. Yousif, Z. Fadel, S. Melhi, F. A. Al-Odail and A. M. Abuelela, Experimental and theoretical analyses of the corrosion inhibition efficacy of new penicillanic acid derivatives for carbon steel in hydrochloric acid environment, *J. Mol. Struct.*, 2025, **1328**, 141282, DOI: 10.1016/j.molstruc.2024.141282.

39 Q. A. Yousif, M. A. Bedair, Z. Fadel, F. Al-Odail and A. M. Abuelela, Evaluating the efficacy of newly synthesized amino acid derivatives as corrosion inhibitors in acidic solutions, *Inorg. Chem. Commun.*, 2024, **164**, 112454, DOI: 10.1016/j.inoche.2024.112454.

40 A. M. Abuelela, J. Kaur, A. Saxena, M. A. Bedair, D. K. Verma and E. Berdimurodov, Electrochemical and DFT studies of Terminalia bellerica fruit extract as an eco-friendly

inhibitor for the corrosion of steel, *Sci. Rep.*, 2023, **13**, 19367, DOI: 10.1038/s41598-023-45283-0.

41 A. Toghan, H. Alhussain, A. Fawzy, M. M. S. Sanad, S. A. Al-Hussain, E. M. Masoud, H. Jiang and A. A. Farag, One-pot synthesis of N′-(thiophen-2-ylmethylene) isonicotinohydrazide Schiff-base as a corrosion inhibitor for C-steel in 1 M HCl: Theoretical, electrochemical, adsorption and spectroscopic inspections, *J. Mol. Struct.*, 2024, **1318**, 139315, DOI: 10.1016/j.molstruc.2024.139315.

42 Y. Lei, R. Dou, H. Zhu, Y. Zhao, L. Zhou, H. Peng and P. Yu, A novel corrosion inhibitor of bis-benzimidazole derivative for mild steel: Synthesis, properties and mechanism investigation, *J. Mol. Struct.*, 2025, **1322**, 140499, DOI: 10.1016/j.molstruc.2024.140499.

43 D. Ma, J. Zhao, L. Zhang, J. Huang, J. Liu and T. Ren, Isatin Schiff bases: A green and sustainable Mg alloys corrosion inhibitor, *Mater. Chem. Phys.*, 2023, **307**, 128163, DOI: 10.1016/j.matchemphys.2023.128163.

44 D. I. Udunwa, O. D. Onukwuli, M. C. Menkiti, S. C. Nwanonenyi, C. B. Ezekannagha and C. O. Aniagor, Experimental, computational, and theoretical studies on the corrosion inhibition potential of green Gongronema latifolium extract as corrosion inhibitor for aluminum alloy in HCl solutions, *J. Mol. Struct.*, 2024, **1302**, 137508, DOI: 10.1016/j.molstruc.2024.137508.

45 Q. A. Yousif, Environmentally sustainable disposal of expired albendazole medication and its role in the protection of mild steel, *IOP Conf. Ser.: Earth Environ. Sci.*, 2021, **790**, 012072, DOI: 10.1088/1755-1315/790/1/012072.

46 M. A. Bedair, Q. A. Yousif, Z. Fadel, S. Melhi, F. A. Al-Odail and A. M. Abuelela, Experimental and theoretical analyses of the corrosion inhibition efficacy of new penicillanic acid derivatives for carbon steel in hydrochloric acid environment, *J. Mol. Struct.*, 2025, **1328**, 141282, DOI: 10.1016/j.molstruc.2024.141282.

47 M. J. Frisch, G. W. Trucks, H. B. Schlegel, G. E. Scuseria, M. A. Robb, J. R. Cheeseman, G. Scalmani, V. Barone, G. A. Petersson, H. Nakatsuji, X. Li, M. Caricato, A. V Marenich, J. Bloino, B. G. Janesko, R. Gomperts, B. Mennucci, H. P. Hratchian, J. V Ortiz, A. F. Izmaylov, J. L. Sonnenberg, D. Williams-Young, F. Ding, F. Lipparini, F. Egidi, J. Goings, B. Peng, A. Petrone, T. Henderson, D. Ranasinghe, V. G. Zakrzewski, J. Gao, N. Rega, G. Zheng, W. Liang, M. Hada, M. Ehara, K. Toyota, R. Fukuda, J. Hasegawa, M. Ishida, T. Nakajima, Y. Honda, O. Kitao, H. Nakai, T. Vreven, K. Throssell, J. A. Montgomery Jr, J. E. Peralta, F. Ogliaro, M. J. Bearpark, J. J. Heyd, E. N. Brothers, K. N. Kudin, V. N. Staroverov, T. A. Keith, R. Kobayashi, J. Normand, K. Raghavachari, A. P. Rendell, J. C. Burant, S. S. Iyengar, J. Tomasi, M. Cossi, J. M. Millam, M. Klene, C. Adamo, R. Cammi, J. W. Ochterski, R. L. Martin, K. Morokuma, O. Farkas, J. B. Foresman, and D. J. Fox, *Gaussian~16 {R} evision {A}.03*, 2016.

48 A. Allouche, Gabedit—A graphical user interface for computational chemistry softwares, *J. Comput. Chem.*, 2011, **32**, 174–182, DOI: 10.1002/jcc.21600.

49 M. A. Bedair, E. H. Alosaimi and S. Melhi, A study of the inhibitive effect for corrosion of steel in 1.0 M HCl using a new nonionic surfactant based on coumarin moiety: chemical, electrochemical and quantum mechanics calculations, *J. Adhes. Sci. Technol.*, 2021, **37**, 1–31, DOI: 10.1080/01694243.2021.2018864.

50 Q. Zhang, Y. Zhang, H. Qi, X. Yang and N. Xu, Integrating experimental and first-principles calculations to evaluate Gleditsiae Sinensis Fructus extract as an eco-friendly corrosion inhibitor for Q235 steel in acidic environment, *J. Mol. Liq.*, 2025, **433**, 127885, DOI: 10.1016/j.molliq.2025.127885.

51 T. Aravinda, D. Kumari, A. S. Sowmyashree, R. Srilatha, K. J. Gururaj, N. Praveen and G. Nagendra, Fmoc centered peptide conjugate as an effective corrosion inhibitor for mild steel in acidic medium: A combined theoretical and experimental approach, *Mater. Today Commun.*, 2025, **47**, 113142, DOI: 10.1016/j.mtcomm.2025.113142.

52 M. A. Bedair, H. M. Elaryian, E. S. Gad, M. Alshareef, A. H. Bedair, R. M. Aboushahba and A. S. Fouda, Insights into the adsorption and corrosion inhibition properties of newly synthesized diazinyl derivatives for mild steel in hydrochloric acid: synthesis, electrochemical, SRB biological resistivity and quantum chemical calculations, *RSC Adv.*, 2023, **13**, 478–498, DOI: 10.1039/D2RA06574F.

53 L. Raisemche, I. Kaabi, T. Douadi, M. Al-Noaimi, A. Alrashed, M. S. Mubarak, N. Elboughdiri, A. Zouaoui and Y. Benguerba, Corrosion inhibition of mild steel in acidic environments: Mechanistic insights and protective effects of azo-cum inhibitor, *J. Environ. Chem. Eng.*, 2024, **12**, 112354, DOI: 10.1016/j.jece.2024.112354.

54 L. Feng, H. Yang and F. Wang, Experimental and theoretical studies for corrosion inhibition of carbon steel by imidazoline derivative in 5% NaCl saturated Ca(OH)2 solution, *Electrochim. Acta*, 2011, **58**, 427–436, DOI: 10.1016/j.electacta.2011.09.063.

55 P. Lowmunkhong, D. Ungthararak and P. Sutthivaiyakit, Tryptamine as a corrosion inhibitor of mild steel in hydrochloric acid solution, *Corros. Sci.*, 2010, **52**, 30–36, DOI: 10.1016/j.corsci.2009.08.039.

56 R. Sattari, G. R. Khayati and E. Darezereshki, Electrochemical-surface and theoretical investigations of the interactions of Salvia officinalis extract as a green and sustainable corrosion inhibitor and zinc cations for corrosion protection of carbon steel in sodium chloride solution, *J. Mol. Liq.*, 2025, **433**, 127962, DOI: 10.1016/j.molliq.2025.127962.

57 H. M. Elaryian, M. A. Bedair, A. H. Bedair, R. M. Aboushahba and A. E.-A. S. Fouda, Corrosion mitigation for steel in acid environment using novel p-phenylenediamine and benzidine coumarin derivatives: synthesis{,} electrochemical{,} computational and SRB biological resistivity, *RSC Adv.*, 2022, **12**, 29350–29374, DOI: 10.1039/D2RA05803K.

58 M. A. Bedair, H. M. Elaryian, A. H. Bedair, R. M. Aboushahba, A. El-Aziz and S. Fouda, Novel coumarin-buta-1,3-diene conjugated donor–acceptor

systems as corrosion inhibitors for mild steel in 1.0 M HCl: Synthesis, electrochemical, computational and SRB biological resistivity, *Inorg. Chem. Commun.*, 2023, **148**, 110304, DOI: 10.1016/j.inoche.2022.110304.

59 J. Jomy and D. Prabhu, Biopolymer Xylan as a novel green corrosion inhibitor for AISI 5140 steel and copper in H2SO4 medium, *J. Taiwan Inst. Chem. Eng.*, 2025, **174**, 106225, DOI: 10.1016/j.jtice.2025.106225.

60 M. M. Kamel, S. N. Abdou, Z. M. Anwar, M. A. Sherif and N. Y. Mostafa, Reusing the expired Ceftazidime drug as an inhibiting agent for zinc metal corrosion in HCl medium, *RSC Adv.*, 2025, **15**, 8506–8522, DOI: 10.1039/D5RA00650C.

61 M. A. Bedair, In-depth assessment of new coumarin derivative based on azo dye and Schiff base as an effective corrosion inhibitor for steel in 1 M HCl solution and anti sulphate reducing bacteria: Insights from computational and experimental techniques, *Inorg. Chem. Commun.*, 2024, **167**, 112693, DOI: 10.1016/j.inoche.2024.112693.

62 K. Dahmani, A. E. M. Ala Allah, Z. Aribou, O. Kharbouch, M. Galai, R. Almeer, M. E. Touhami, Y. Ramli, M. Cherkaoui, A. Chaouiki and Y. G. Ko, Imidazole derivative for corrosion protection: A comprehensive theoretical and experimental study on mild steel in acidic environments, *Colloids Surf., A*, 2025, **704**, 135376, DOI: 10.1016/j.colsurfa.2024.135376.

63 V. M. dos Santos, C. M. Fernandes, M. T. G. Sampaio, K. R. Lucio, J. A. C. Velasco, F. L. Salazar, L. X. Alvarez, H. Lgaz and E. A. Ponzio, Integrating experimental and *ab initio* DFT approaches to evaluate chalcone derivatives as corrosion inhibitors for mild steel in acidic environment, *J. Mol. Liq.*, 2025, **418**, 126704, DOI: 10.1016/j.molliq.2024.126704.

64 A. M. Abuelela, M. A. Bedair, W. M. Zoghaib, L. D. Wilson and T. A. Mohamed, Molecular structure and mild steel/HCl corrosion inhibition of 4,5-Dicyanoimidazole: Vibrational, electrochemical and quantum mechanical calculations, *J. Mol. Struct.*, 2021, **1230**, 129647, DOI: 10.1016/j.molstruc.2020.129647.

65 H. M. Elaryian, M. A. Bedair, A. H. Bedair, R. M. Aboushahba and A. E.-A. S. Fouda, Synthesis, characterization of novel coumarin dyes as corrosion inhibitors for mild steel in acidic environment: Experimental, theoretical, and biological studies, *J. Mol. Liq.*, 2022, **346**, 118310, DOI: 10.1016/j.molliq.2021.118310.

66 M. M. M. Madkhali, F. O. Sefrji, M. A. Aljowni, K. B. Alomari, J. Qurban, M. M. Abualnaja, A. A. Alfi and N. M. El-Metwaly, Multifunctional Properties of 2-Amino-6-hydroxy-4-(4-hydroxy-3-methoxyphenyl)-4H-chromene-3-carbonitrile: An innovative strategy for corrosion inhibition and antimicrobial activity, *Surf. Interfaces*, 2025, **65**, 106450, DOI: 10.1016/j.surfin.2025.106450.

67 M. A. Gebril, M. A. Bedair, S. A. Soliman, M. F. Bakr and M. B. I. Mohamed, Experimental and computational studies of the influence of non-ionic surfactants with coumarin moiety as corrosion inhibitors for carbon steel in 1.0 M HCl, *J. Mol. Liq.*, 2022, **349**, 118445, DOI: 10.1016/j.molliq.2021.118445.

68 M. Ouakki, Z. Aribou, E. Ech-chihbi, K. Mzioud, O. Kharbouch, B. Srhir and M. Cherkaoui, Comparative study of natural and synthetic polymers as corrosion inhibitors for mild steel in 1.0 M HCl solution, *Colloids Surf., A*, 2025, **723**, 137355, DOI: 10.1016/j.colsurfa.2025.137355.

69 A. Gangan, M. ElSabbagh, M. A. Bedair, H. M. Ahmed, M. El-Sabbah, S. M. El-Bahy and A. Fahmy, Influence of pH values on the electrochemical performance of low carbon steel coated by plasma thin SiO C films, *Arabian J. Chem.*, 2021, **14**, 103391, DOI: 10.1016/j.arabjc.2021.103391.

70 M. T. Alotaibi, Synthesis, characterization and evaluation of a novel thiazolidinone derivative as a corrosion inhibitor for C38 steel in 1 M HCl medium: experimental and DFT analysis, *J. Mol. Liq.*, 2025, **433**, 127757, DOI: 10.1016/j.molliq.2025.127757.

71 I. Ahmad, M. Yadav, S. Zamindar and P. Banerjee, Detailed experimental and quantum chemical investigation on polysaccharide derived from Gellan Gum as a potent and green corrosion inhibitor for mild steel in 15 % HCl, *Int. J. Biol. Macromol.*, 2025, **317**, 144607, DOI: 10.1016/j.ijbiomac.2025.144607.

72 M. A. M. Alwi, M. N. Ahmad, B. M. Piah, H. Pauzi and E. Normaya, Synthesis of bioactive Schiff base thiosemicarbazone analogs with quinoline for high-performance copper corrosion inhibition: Insights from RSM-assisted EIS, XPS, DFT, and MD studies, *J. Mol. Struct.*, 2025, **1345**, 142961, DOI: 10.1016/j.molstruc.2025.142961.

73 M. A. Abbas, E. I. Arafa, M. A. Bedair, A. S. Ismail, O. E. El-Azabawy, S. A. Baker and H. I. Al-Shafey, Synthesis, Characterization, Thermodynamic Analysis and Quantum Chemical Approach of Branched N, N′-bis(p-hydroxybenzoyl)-Based Propanediamine and Triethylenetetramine for Carbon Steel Corrosion Inhibition in Hydrochloric Acid Medium, *Arabian J. Sci. Eng.*, 2023, **48**, 7463–7484, DOI: 10.1007/s13369-022-07520-y.

74 A. M. Abuelela, J. Kaur, A. Saxena, M. A. Bedair, D. K. Verma and E. Berdimurodov, Electrochemical and DFT studies of Terminalia bellerica fruit extract as an eco-friendly inhibitor for the corrosion of steel, *Sci. Rep.*, 2023, **13**, 19367, DOI: 10.1038/s41598-023-45283-0.

75 A. Elaraby, K. F. Qasim, S. K. Mohamed, E. A. El-Sharkawy and S. Abdelhamed, Multi-scale quantum (DFT, MCs and MDs) insights and electrochemical validation of di-imine Schiff base inhibitor for carbon steel corrosion control in 1 M HCl solution, *Appl. Mater. Today*, 2025, **42**, 102615, DOI: 10.1016/j.apmt.2025.102615.

76 E. S. Gad, M. A. Abbas, M. A. Bedair, O. E. El-Azabawy and S. M. Mukhtar, Synthesis and applications of novel Schiff base derivatives as corrosion inhibitors and additives for improvement of reinforced concrete, *Sci. Rep.*, 2023, **13**, 15091, DOI: 10.1038/s41598-023-41165-7.

77 M. Ragab and M. A. Bedair, The effect of permanent magnet stirring on the corrosion resistance of Sn-2.0Ag-0.5Cu-2Zn solder alloys in NaCl solution, *Mater. Chem. Phys.*, 2023, **302**, 127774, DOI: 10.1016/j.matchemphys.2023.127774.

78 R. Haldhar, C. J. Raorane, V. Bachhar, K. P. Katin, E. Berdimurodov, G. A. Shazly and S.-C. Kim, Dual-functional Quercus palustris leaves extract as a sustainable corrosion inhibitor for low-carbon steel and its biomedical potential: Electrochemical, biological, and computational insights, *Sustainable Mater. Technol.*, 2025, **44**, e01378, DOI: 10.1016/j.susmat.2025.e01378.

79 A. M. Abuelela, M. A. Bedair, E. S. Gad, Y. F. El-Aryan, W. A. A. Arafa, A. K. Mourad, H. Nady and S. Eid, Exploring the synthesis, characterization, and corrosion inhibition of new tris-thiosemicarbazone derivatives for acidic steel settings using computational and experimental studies, *Sci. Rep.*, 2024, **14**, 13310, DOI: 10.1038/s41598-024-64199-x.

80 Y. Youssefi, S. Kharchouf, N. Asoufar, L. Oucheikh, O. Ouani, A. Ansari, A. Oubair, D. Chebabe, E. H. Mabrouk, Z. Faska and M. Znini, Synthesis, characterization and evaluation of new α-arylidene-γ-lactams derivatives as corrosion inhibitor for carbon steel in in 1M HCl medium: Combination of experimental, surface morphological and computational insights, *J. Mol. Struct.*, 2025, **1342**, 142766, DOI: 10.1016/j.molstruc.2025.142766.

81 M. A. Bedair, M. M. B. El-Sabbah, A. S. Fouda and H. M. Elaryian, Synthesis, electrochemical and quantum chemical studies of some prepared surfactants based on azodye and Schiff base as corrosion inhibitors for steel in acid medium, *Corros. Sci.*, 2017, **128**, 54–72, DOI: 10.1016/j.corsci.2017.09.016.

82 W. Ettahiri, M. Ait Lahcen, D. Fadili, A. S. Alanazi, Z. Rais, M. M. Alanazi, S. K. Wiedmer, A. Baouid and M. Taleb, Regio- and chemoselective synthesis of triazolobenzodiazepines as efficient corrosion inhibitors for mild steel: Insights from experimental and multiscale theoretical approaches, *Colloids Surf., A*, 2025, **723**, 137356, DOI: 10.1016/j.colsurfa.2025.137356.

83 M. Bedair, M. Metwally, S. Soliman, A. Al-Sabagh, A. Salem and T. Mohamed, Extracts Of Mint And Tea As Green Corrosion Inhibitors For Mild Steel In Hydrochloric Acid Solution, *Al-Azhar Bull. Sci.*, 2015, **26**, 1–14, DOI: 10.21608/absb.2015.23766.

84 Z. Wei, Y. Zhang, H. Xia, L. Ni, W. Wu, X. Wang and H. Quan, Catechol derivative as a novel bio-based corrosion inhibitor for carbon steel in 1M HCl solution: Synthesis, experiments, and theoretical studies, *J. Mol. Struct.*, 2025, **1342**, 142687, DOI: 10.1016/j.molstruc.2025.142687.

85 N. B. Iroha, C. U. Dueke-Eze, V. C. Anadebe, N. J. Maduelosi, R. Thomas and E. E. Ebenso, Assessment of a new benzylidene-based corrosion inhibitor for X60 carbon steel in 1 M HCl medium: Experimental and computational studies, *Results Surf. Interfaces*, 2025, **19**, 100510, DOI: 10.1016/j.rsurfi.2025.100510.

86 A. Kumar, B. Bhattacharya and C. Das, Studies on the inhibitive effect of ferrozine on the corrosion of mild steel in hydrochloric acid, *J. Taiwan Inst. Chem. Eng.*, 2025, **174**, 106221, DOI: 10.1016/j.jtice.2025.106221.

87 A. M. Ashmawy, R. Said, I. A. Naguib, B. Yao and M. A. Bedair, Anticorrosion Study for Brass Alloys in Heat Exchangers during Acid Cleaning Using Novel Gemini Surfactants Based on Benzalkonium Tetrafluoroborate, *ACS Omega*, 2022, **7**, 17849–17860, DOI: 10.1021/acsomega.2c01119.

88 M. A. Abbas, M. A. Bedair, O. E. El-Azabawy, E. S. Gad, M. A. Abbas, M. A. Bedair, O. E. El-Azabawy and E. S. Gad, Anticorrosion Effect of Ethoxylate Sulfanilamide Compounds on Carbon Steel in 1 M Hydrochloric Acid: Electrochemical and Theoretical Studies, *ACS Omega*, 2021, **6**, 15089–15102, DOI: 10.1021/acsomega.1c01274.

89 M. Y. Chaudhary, M. Gupta, Y. S. Sharma, P. Bansal, S. Kaushik, R. Kanojia, M. K. Gautam and S. Yadav, Benzyl triphenyl phosphonium bromide as a corrosion inhibitor: A multifaceted study on aluminium protection in acidic environment, *J. Ionic Liq.*, 2025, **5**, 100152, DOI: 10.1016/j.jil.2025.100152.

90 T. Liu, X. Li, P. Du, L. Qiu, Y. Chen and S. Deng, Amphoteric surfactant of dodecyl dimethyl betaine as a highly efficient inhibitor for the corrosion of steel in HCl solution, *J. Mol. Struct.*, 2025, **1340**, 142566, DOI: 10.1016/j.molstruc.2025.142566.

91 M. A. Bedair, A. M. Abuelela, M. Alshareef, M. Owda and E. M. Eliwa, Ethyl ester/acyl hydrazide-based aromatic sulfonamides: facile synthesis, structural characterization, electrochemical measurements and theoretical studies as effective corrosion inhibitors for mild steel in 1.0 M HCl, *RSC Adv.*, 2023, **13**, 186–211, DOI: 10.1039/D2RA05939H.

92 Q. A. Yousif, Z. Fadel, A. M. Abuelela, E. H. Alosaimi, S. Melhi and M. A. Bedair, Insight into the corrosion mitigation performance of three novel benzimidazole derivatives of amino acids for carbon steel (X56) in 1 M HCl solution, *RSC Adv.*, 2023, **13**, 13094–13119, DOI: 10.1039/D3RA01837G.

93 M. A. Al-Qudah, T. T. Bataineh, F. M. Abu Orabi, S. T. Abu-Orabi, G. M. Al-Mazaideh and A. I. Alakhras, Acteoside: a novel green inhibitor for the corrosion of copper in 1.0 M HNO 3 solution: experimental and theoretical investigation, *RSC Adv.*, 2025, **15**, 9335–9347, DOI: 10.1039/D5RA01657F.

94 C. G. Vaszilcsin, M. V. Putz, A. Kellenberger and M. L. Dan, On the evaluation of metal-corrosion inhibitor interactions by adsorption isotherms, *J. Mol. Struct.*, 2023, **1286**, 135643, DOI: 10.1016/j.molstruc.2023.135643.

95 S. Melhi, M. A. Bedair, E. H. Alosaimi, A. A. O. Younes, W. H. El-Shwiniy and A. M. Abuelela, Effective corrosion inhibition of mild steel in hydrochloric acid by newly synthesized Schiff base nano Co(II) and Cr(III) complexes: spectral, thermal, electrochemical and DFT (FMO, NBO) studies, *RSC Adv.*, 2022, **12**, 32488–32507, DOI: 10.1039/D2RA06571A.

96 S. S. Alarfaji, I. H. Ali, M. Z. Bani-Fwaz and M. A. Bedair, Synthesis and Assessment of Two Malonyl Dihydrazide Derivatives as Corrosion Inhibitors for Carbon Steel in Acidic Media: Experimental and Theoretical Studies, *Molecules*, 2021, **26**, 3183, DOI: 10.3390/molecules26113183.

97 M. A. Abbas, E. I. Arafa, E. S. Gad, M. A. Bedair, O. E. El-Azabawy and H. I. Al-Shafey, Performance assessment by experimental and Theoretical approaches of newly synthetized benzyl amide derivatives as corrosion inhibitors for carbon steel in 1.0 M hydrochloric acid environment, *Inorg. Chem. Commun.*, 2022, **143**, 109758, DOI: 10.1016/j.inoche.2022.109758.

98 A. Kokalj, On the alleged importance of the molecular electron-donating ability and the HOMO–LUMO gap in corrosion inhibition studies, *Corros. Sci.*, 2021, **180**, 109016, DOI: 10.1016/j.corsci.2020.109016.

99 M. A. Deyab, Q. Mohsen and O. A. A. El-Shamy, Investigation of the energy gap and anti-corrosion activities of triethanolamine lauryl sulfate for carbon steel in 1.0 M HCl using DFT theory and electrochemical studies, *Colloids Surf., A*, 2024, **702**, 135024, DOI: 10.1016/j.colsurfa.2024.135024.

100 I. Lukovits, E. Kálmán, F. Zucchi, E. Kálmán and F. Zucchi, Corrosion Inhibitors—Correlation between Electronic Structure and Efficiency, *Corrosion*, 2001, **57**, 3–8, DOI: 10.5006/1.3290328.

101 S. Yesudass, L. O. Olasunkanmi, I. Bahadur, M. M. Kabanda, I. B. Obot and E. E. Ebenso, Experimental and theoretical studies on some selected ionic liquids with different cations/anions as corrosion inhibitors for mild steel in acidic medium, *J. Taiwan Inst. Chem. Eng.*, 2016, **64**, 252–268, DOI: 10.1016/j.jtice.2016.04.006.

102 H. M. Abd El-Lateef, K. Shalabi and A. H. Tantawy, Corrosion inhibition of carbon steel in hydrochloric acid solution using newly synthesized urea-based cationic fluorosurfactants: experimental and computational investigations, *New J. Chem.*, 2020, **44**, 17791–17814, DOI: 10.1039/D0NJ04004E.

103 M. Goyal, H. Vashist, S. Kumar, I. Bahadur, F. Benhiba and A. Zarrouk, Acid corrosion inhibition of ferrous and non-ferrous metal by nature friendly Ethoxycarbonylmethyltriphenylphosphonium Bromide (ECMTPB): Experimental and MD simulation evaluation, *J. Mol. Liq.*, 2020, **315**, 113705, DOI: 10.1016/j.molliq.2020.113705.

104 K. Shalabi, A. M. Helmy, A. H. El-Askalany and M. M. Shahba, New pyridinium bromide mono-cationic surfactant as corrosion inhibitor for carbon steel during chemical cleaning: Experimental and theoretical studies, *J. Mol. Liq.*, 2019, **293**, 111480, DOI: 10.1016/j.molliq.2019.111480.

105 A. Dehghani, A. H. Mostafatabar, G. Bahlakeh and B. Ramezanzadeh, A detailed study on the synergistic corrosion inhibition impact of the Quercetin molecules and trivalent europium salt on mild steel; electrochemical/surface studies, DFT modeling, and MC/MD computer simulation, *J. Mol. Liq.*, 2020, **316**, 113914, DOI: 10.1016/j.molliq.2020.113914.

106 S. S. Malhotra, M. Kumar, M. K. Gupta and A. Ansari, Theoretical exploration of copper based electrolytes for third generation dye sensitized solar cells, *Mater. Today Commun.*, 2024, **39**, 109208, DOI: 10.1016/j.mtcomm.2024.109208.

107 S. S. Malhotra, M. Ahmed, M. Kumar, M. A. Amin, S. M. El-Bahy, Z. M. El-Bahy, R. K. Mohapatra and A. Ansari, Theoretical exploration of a di-carbazole based dye for 3rd generation dye-sensitized solar cells, *Mater. Today Commun.*, 2024, **41**, 110182, DOI: 10.1016/j.mtcomm.2024.110182.

108 M. Govindarajan, M. Karabacak, S. Periandy and D. Tanuja, Spectroscopic (FT-IR, FT-Raman, UV and NMR) investigation and NLO, HOMO–LUMO, NBO analysis of organic 2,4,5-trichloroaniline, *Spectrochim. Acta, Part A*, 2012, **97**, 231–245, DOI: 10.1016/j.saa.2012.06.014.

109 M. A. Bedair, A. M. Abuelela, W. M. Zoghaib and T. A. Mohamed, Molecular structure, tautomer's, reactivity and inhibition studies on 6-Methyl-2-thiouracil for mild steel corrosion in aqueous HCl (1.00 M): Experimental and Theoretical Studies, *J. Mol. Struct.*, 2021, **1244**, 130927, DOI: 10.1016/j.molstruc.2021.130927.

110 M. A. Abbas and M. A. Bedair, Adsorption and Computational Studies for Evaluating the Behavior of Silicon Based Compounds as Novel Corrosion Inhibitors of Carbon Steel Surfaces in Acidic Media, *Z. Phys. Chem.*, 2019, **233**, 225–254, DOI: 10.1515/zpch-2018-1159.

111 M. Kumar, A. K. Talakkal, R. K. Mohapatra and A. Ansari, Photophysical properties of four-membered BN3 heterocyclic compounds: theoretical insights, *J. Mol. Model.*, 2023, **29**, 336, DOI: 10.1007/s00894-023-05731-0.

112 M. Ahmed, M. K. Gupta and A. Ansari, DFT and TDDFT exploration on the role of pyridyl ligands with copper toward bonding aspects and light harvesting, *J. Mol. Model.*, 2023, **29**, 358, DOI: 10.1007/s00894-023-05765-4.

113 O. Yadav, M. Ansari and A. Ansari, Electronic structures, bonding aspects and spectroscopic parameters of homo/hetero valent bridged dinuclear transition metal complexes, *Spectrochim. Acta, Part A*, 2022, **278**, 121331, DOI: 10.1016/j.saa.2022.121331.

114 M. Kumar, M. Ansari and A. Ansari, Electronic, geometrical and photophysical facets of five coordinated porphyrin N-heterocyclic carbene transition metals complexes: A theoretical study, *Spectrochim. Acta, Part A*, 2023, **284**, 121774, DOI: 10.1016/j.saa.2022.121774.

115 R. K. Mohapatra, M. Azam, P. K. Mohapatra, A. K. Sarangi, M. Abdalla, L. Perekhoda, O. Yadav, S. I. Al-Resayes, K. Jong-Doo, K. Dhama, A. Ansari, V. Seidel, S. Verma and M. K. Raval, Computational studies on potential new anti-Covid-19 agents with a multi-target mode of action, *J. King Saud Univ., Sci.*, 2022, **34**, 102086, DOI: 10.1016/j.jksus.2022.102086.

116 Monika and A. Ansari, Electronic structures and energetic of metal(II)-superoxo species: a DFT exploration, *Struct.*

Chem., 2023, **34**, 825–835, DOI: **10.1007/s11224-022-02030-x**.

117 O. Yadav, M. Kumar, H. Mittal, K. Yadav, V. Seidel and A. Ansari, Theoretical exploration on structures, bonding aspects and molecular docking of α-aminophosphonate ligated copper complexes against SARS-CoV-2 proteases, *Front. Pharmacol*, 2022, **13**, 982484, DOI: **10.3389/fphar.2022.982484**.

118 M. Kumar, M. K. Gupta, M. Ansari and A. Ansari, C–H bond activation by high-valent iron/cobalt–oxo complexes: a quantum chemical modeling approach, *Phys. Chem. Chem. Phys.*, 2024, **26**, 4349–4362, DOI: **10.1039/D3CP05866B**.

119 S. Raheem, T. Jan, A. Qayum, O. Yadav, M. Mustafa, A. Ansari, G. Mustafa Peerzada, S. K. Singh and M. Ahmad Rizvi, Crystal Structure, quantum chemical analysis and apoptotic propensity of diaryl substituted α-aminophosphonates as selected C P bonded systems, *Polyhedron*, 2023, **244**, 116597, DOI: **10.1016/j.poly.2023.116597**.

120 M. A. Bedair, A novel coumarin-azo Schiff base for dual corrosion inhibition for steel in acidic environments and anti-SRB protection: Experimental and computational insights, *Results Surf. Interfaces*, 2025, **19**, 100511, DOI: **10.1016/j.rsurfi.2025.100511**.